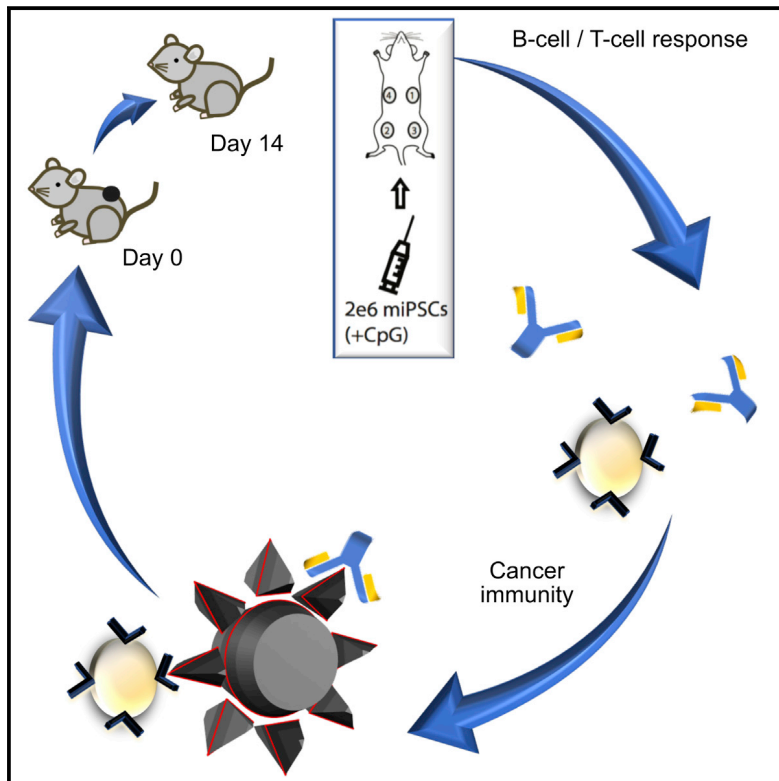


Cell Stem Cell

Autologous iPSC-Based Vaccines Elicit Anti-tumor Responses *In Vivo*

Graphical Abstract



Authors

Nigel G. Kooreman, Youngkyun Kim, Patricia E. de Almeida, ..., Ronald Levy, Mark M. Davis, Joseph C. Wu

Correspondence

levy@stanford.edu (R.L.),
mmdavis@stanford.edu (M.M.D.),
joewu@stanford.edu (J.C.W.)

In Brief

Wu and colleagues show that cancer immunity against multiple types of cancer can be achieved using an easily generable iPSC-based cancer vaccine. This immunity is based on overlapping epitopes between iPSCs and cancer cells and can also be achieved by reactivating the immune system as an adjuvant immunotherapy.

Highlights

- Irradiated iPSCs prevent tumor growth in murine models of breast, lung, and skin cancer
- iPSC vaccines target shared antigens between iPSCs and cancer cells
- iPSC vaccines promote a humoral and cell-mediated anti-tumor immune profile
- As an adjuvant cancer therapy, iPSC vaccination can reactivate the immune system

Autologous iPSC-Based Vaccines Elicit Anti-tumor Responses *In Vivo*

Nigel G. Kooreman,^{1,2,3,4,12} Youngkyun Kim,^{1,2,3,7,12} Patricia E. de Almeida,^{1,2,3} Vittavat Termglinchan,^{1,2,3} Sebastian Diecke,^{8,9,10} Ning-Yi Shao,^{1,2,3} Tzu-Tang Wei,^{1,2,3} Hyoju Yi,^{1,2,3,7} Devaveena Dey,^{1,2,3} Raman Nelakanti,^{1,2,3} Thomas P. Brouwer,^{1,2,3,4} David T. Paik,^{1,2,3} Idit Barfi,⁵ Arnold Han,⁶ Paul H.A. Quax,⁴ Jaap F. Hamming,⁴ Ronald Levy,^{5,*} Mark M. Davis,^{6,*} and Joseph C. Wu^{1,2,3,11,*}

¹Institute for Stem Cell Biology and Regenerative Medicine, Stanford University School of Medicine, Stanford, CA 94305, USA

²Stanford Cardiovascular Institute of Medicine, Stanford University School of Medicine, Stanford, CA 94305, USA

³Department of Radiology, Stanford University School of Medicine, Stanford, CA 94305, USA

⁴Department of Surgery, Leiden University Medical Center, Leiden 2333 ZA, the Netherlands

⁵Stanford Cancer Institute, Stanford University School of Medicine, Stanford, CA 94305, USA

⁶Institute for Immunity, Transplantation, and Infection, Stanford University School of Medicine, Stanford, CA 94305, USA

⁷Convergent Research Consortium for Immunologic Disease, Seoul St. Mary's Hospital, Catholic University of Korea, Seoul 06591, Korea

⁸Max Delbrück Center for Molecular Medicine in the Helmholtz Association (MDC), Robert-Rossle Strasse 10, 13125 Berlin, Germany

⁹DZHK (German Centre for Cardiovascular Research), Partner Site, Berlin, Germany

¹⁰Berlin Institute of Health (BIH), Berlin, Germany

¹¹Lead Contact

¹²These authors contributed equally

*Correspondence: levy@stanford.edu (R.L.), mmdavis@stanford.edu (M.M.D.), joewu@stanford.edu (J.C.W.)

<https://doi.org/10.1016/j.stem.2018.01.016>

SUMMARY

Cancer cells and embryonic tissues share a number of cellular and molecular properties, suggesting that induced pluripotent stem cells (iPSCs) may be harnessed to elicit anti-tumor responses in cancer vaccines. RNA sequencing revealed that human and murine iPSCs express tumor-associated antigens, and we show here a proof of principle for using irradiated iPSCs in autologous anti-tumor vaccines. In a prophylactic setting, iPSC vaccines prevent tumor growth in syngeneic murine breast cancer, mesothelioma, and melanoma models. As an adjuvant, the iPSC vaccine inhibited melanoma recurrence at the resection site and reduced metastatic tumor load, which was associated with fewer Th17 cells and increased CD11b⁺GR1^{hi} myeloid cells. Adoptive transfer of T cells isolated from vaccine-treated tumor-bearing mice inhibited tumor growth in unvaccinated recipients, indicating that the iPSC vaccine promotes an antigen-specific anti-tumor T cell response. Our data suggest a generalizable strategy for multiple types of cancer that could prove highly valuable in clinical immunotherapy.

INTRODUCTION

Nearly a century ago, researchers observed that immunization with embryonic materials led to the rejection of transplanted tumors (Brewer et al., 2009). More recently, studies identified shared transcriptome profiles and antigens on various tumor cells and embryonic cells (Ben-Porath et al., 2008; Ghosh

et al., 2011). This has led to the hypothesis that embryonic stem cells (ESCs) could be used as immunization agents to promote an anti-tumor response. A major advantage of whole-cell vaccination over traditional vaccines, which consist of inactivated organisms or protein products, is that a broad range of antigens can be presented to T cells, including unknown antigens (Palena et al., 2006; Yaddanapudi et al., 2012). However, the use of fetal and embryonic materials as vaccines to induce anti-tumor immunity has not yet advanced beyond animal models, owing largely to ethical challenges surrounding these therapies.

Since the discovery of induced pluripotent stem cells (iPSCs) (Takahashi et al., 2007; Takahashi and Yamanaka, 2006), pluripotent cells from a patient's own tissues can be created that share nearly identical gene expression and surface markers profiles with ESCs (Bock et al., 2011; Mallon et al., 2013, 2014; Soldner et al., 2009), circumventing a major ethical roadblock. Additionally, the tumorigenic (Kooreman and Wu, 2010; Lee et al., 2013) and immunogenic (de Almeida et al., 2014; Zhao et al., 2011) properties of iPSCs with autologous transplantation suggest potential efficacy in cancer vaccination. Importantly, autologous iPSCs may provide a more accurate and representative panel of patient's tumor immunogens than non-autologously derived ESCs. Here, we test the hypothesis that iPSCs may work as a whole-cell-based vaccine that presents T cells with a broad heterogeneity in cancer-related epitopes.

RESULTS

Human and Murine iPSCs Express Tumor-Specific and Tumor-Associated Antigens

We first performed RNA sequencing on 11 different human iPSC clones to compare expression profiles from a selected cancer-related gene list to human ESCs (hESCs), cancer tissues, and healthy tissues (Figure S1A). Based on this gene

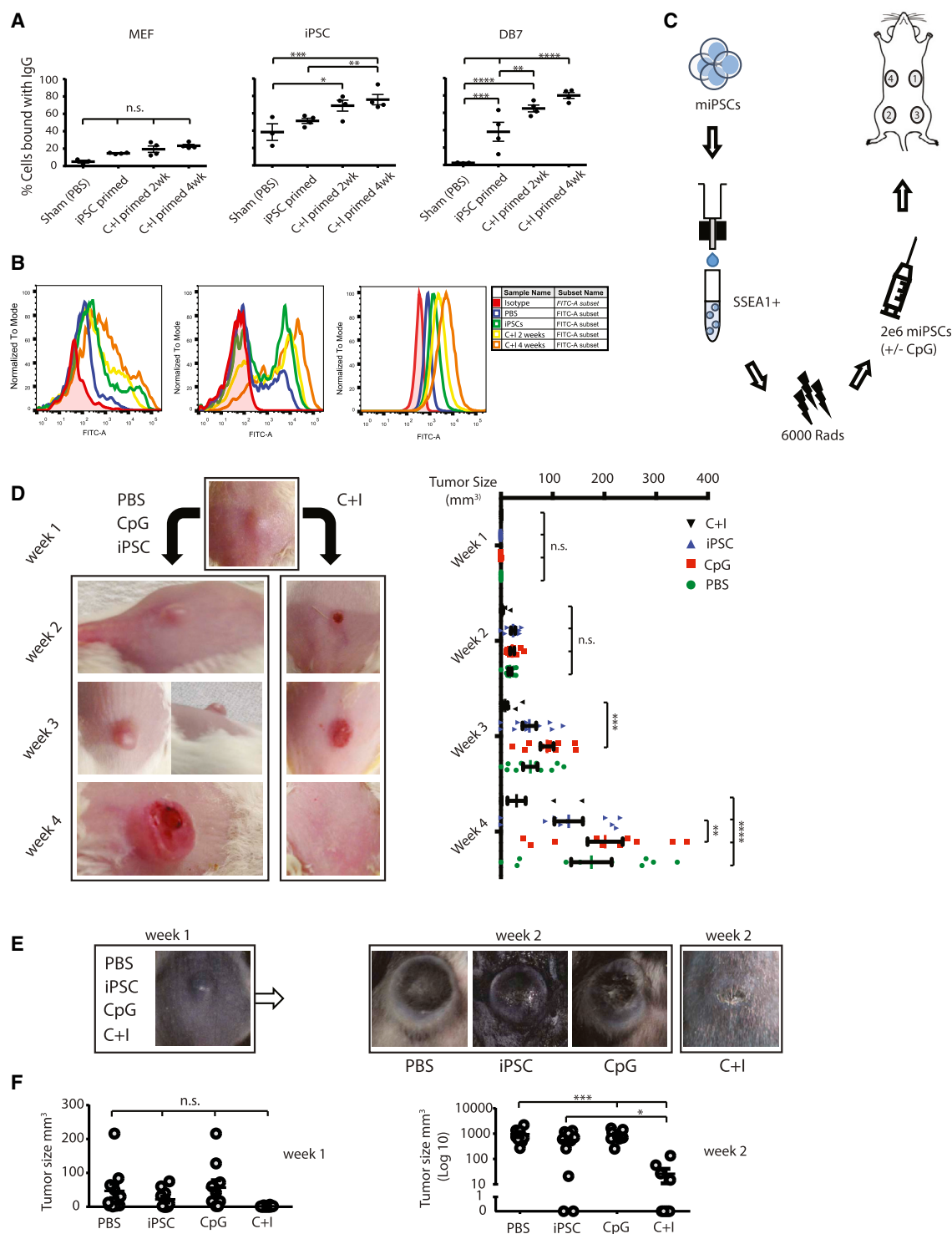


Figure 1. Assessing the Optimal Vaccination Schedule, followed by Successful Prophylactic Treatment of Breast Cancer and Melanoma in Mice

(A) Optimal vaccination was set to C+I vaccination for 4 weeks, as assessed by percent IgG binding to DB7, without a significant increase in non-specific mouse embryonic feeder (MEF) binding ($n = 3$ control animals, $n = 4$ iPSC primed animals, $n = 4$ C+I primed 2 week, and $n = 4$ C+I primed 4 week animals, mean \pm SEM, ANOVA with Tukey's multiple comparison test).

(B) Representative FACS plot of serum IgG binding of PBS 4-week, iPSC 4-week, C+I 2-week, or C+I 4-week vaccinated mice to embryonic fibroblasts, iPSCs, and DB7 cancer cells. As a control sample for differentiated cells, a partly differentiated cell culture was included in the analysis. This is shown by IgG-positive and negative cells, indicating that the IgG binding is specific to the undifferentiated portion of the analyzed cells. C+I 4-week-vaccinated mice showed the best IgG binding to DB7 breast cancer cells.

(legend continued on next page)

list, we found human iPSCs cluster with hESCs and the cancer tissues, revealing important gene expression overlap in cancer genes between different cancer types and iPSCs. The upregulation of a subset of these genes was then also validated in murine iPSCs and ESCs (Figure S1B). These findings suggest the possibility of using iPSCs in different species to prime the host in developing immunity against known and, perhaps, unknown tumor-specific antigens (TSAs) and tumor-associated antigens (TAAs).

iPSC-Vaccine-Primed Mice Mount Strong B and T Cell Responses against Breast Cancer *In Vitro* and *In Vivo*

Using FVB strain iPSCs (Figures S2A and S2D) and the adjuvant CpG, proven to be successful in tumor vaccination (Gilkerson et al., 1998; Goldstein et al., 2011; Mor et al., 1997; Mukherjee et al., 2007), we observed an effective immune response to a murine breast cancer (DB7) with a CpG and iPSCs (C+I) combination. In brief, we first established the effect of CpG and an optimal vaccination schedule. We primed FVB mice with iPSCs or C+I for 2 weeks or 4 weeks and found the strongest *in vitro* T cell responses to DB7 tumor lysate in the C+I 4-week group (Figures S2E and S2F). In addition, a vaccination schedule of 4 weeks with the C+I combination resulted in the highest immunoglobulin G (IgG) binding ($80.0\% \pm 3.4\%$) to DB7 and was therefore used for subsequent vaccination rounds (Figures 1A and 1B). After optimizing the schedule (Figure 1C), we proceeded with the vaccination of 40 FVB mice divided into four groups: (1) PBS, (2) CpG only, (3) iPSCs only, and (4) C+I. After four once-weekly vaccinations, 5×10^4 DB7 cancer cells were injected subcutaneously, and tumor size was monitored using caliper measurement. After 1 week, all mice presented with a similar lesion at the injection site that regressed in 7 out of 10 C+I-treated mice and progressed to larger tumors in the other groups (Figures 1D, S3A, and S3B). Four weeks after tumor inoculation, five mice per group were sacrificed to analyze the immune profiles in blood, spleen, and draining lymph nodes (dLNs). The other five mice per group were used for long-term survival studies for up to 1 year. Most were sacrificed in the first 2 weeks after the end of the experiment when their tumor exceeded 1 cm^3 . However, two mice in the C+I treatment group survived 1 year and had antibody titers against iPSCs and DB7 similar to the start of the experiment and were able to fully reject 5×10^4 cancer cells upon reintroduction (Figures S3C and S3D). The control mice in this experiment, primed with iPSC-derived endothelial cells, were unable to mount IgG responses to the DB7 cell line, thereby ruling out the possibility that the culturing conditions with FBS-containing media could be responsible for the cross-reactivity or endogenous murine leukemia viral antigens.

C+I Vaccination Provides Breast Cancer and Melanoma Immunity by Upregulating Antigen Presentation and T-Helper/Cytotoxic T Cell Activity

To test the effectiveness of our vaccine in targeting multiple cancer types, an additional experiment was performed using the melanoma cell line B16F0, which is syngeneic to the C57BL/6 mouse strain. C57BL/6 iPSCs were generated (Figures S2B and S2D), and 40 mice were again divided into PBS, CpG, iPSCs, and C+I groups and treated for 4 weeks. Following this, 5×10^4 B16F0 cells were subcutaneously injected in the lower back. Tumor growth assessment by caliper measurement showed significantly lower tumor progression by week 2 in the C+I group (Figures 1E, 1F, S3E, and S3F). Due to large tumor sizes in the control groups, the mice were sacrificed 2 weeks after tumor injection. Afterward, the immune cell profiles in blood, dLNs, and spleens were analyzed using flow cytometry. Cytometric analysis showed a significant decrease in $\text{CD4}^+\text{CD25}^+\text{FoxP3}^+$ regulatory T cells (T-regs) in blood and an increase in effector/memory helper T cells in dLNs 2 weeks after tumor injections in C57BL/6 mice (Figures 2A and 2B), as well as increased percentages of mature antigen-presenting cells (APCs) (Figure 2C).

At 4 weeks, FVB mice in the C+I-vaccinated group had significant increases in the effector/memory cytotoxic T cells in the spleen and dLNs (Figures 2D and 2F). The tumor specificity of these cytotoxic T cells was further confirmed by increased secretion of interferon- γ (IFN- γ) by splenocytes isolated from C+I-vaccinated mice in response to DB7 tumor lysate (Figures 3A, 3B, S4A, and S4B). As with the C57BL/6 mice, upregulation of mature APCs and helper T cells was also seen in dLNs of FVB mice (Figures 2E and 2F). Both mouse strains remained healthy throughout the study and showed no signs of autoimmune responses due to the vaccine in serum and in tissues (Figures S4C–S4F). Lastly, the effectiveness of the C+I vaccine was assessed in the more clinically relevant orthotopic model of breast cancer. Significant tumor size differences were seen as early as 1 week after orthotopic transfer of cancer cells in C+I-vaccinated mice compared to vehicle control, followed by further tumor reduction over the course of 3 weeks (Figures 3C and 3E). Using an additional group of orthotopic breast cancer mice, *in vivo* tumor specificity was tested by adoptively transferring splenocytes from C+I vaccinated or vehicle (PBS+CpG) vaccinated mice into these tumor-bearing mice (Figure 3D). This resulted in a significant reduction of tumor sizes in the C+I-vaccinated group compared to the vehicle-vaccinated group (Figure 3F).

Tumor Immunity in C+I-Vaccinated Mice Is the Result of Shared Epitopes between iPSCs and Cancer Cells

To test whether the C+I vaccine provides immunity against shared epitopes between iPSCs and cancer cells, we performed additional experiments to assess two-way immunity

(C) Schema showing vaccine preparation consists of sorting murine iPSCs for pluripotency, irradiation, resuspension in adjuvant solution, and subcutaneous injection in the flank (sites 1–4).

(D) Vaccination of FVB mice with C+I resulted in a complete rejection of the cancer cells in 7 out of 10 mice by 4 weeks and overall reductions in DB7 tumor size ($n = 10$ per group; representative images; left). Quantification of the data presented (right).

(E) Vaccination of C57BL/6 mice with C+I resulted in significant reduction of melanoma sizes initiated by the aggressive B16F0 melanoma cell line by week 2 ($n = 8$ PBS, $n = 9$ iPSC primed, $n = 10$ CpG primed, and $n = 9$ C+I primed).

(F) Quantification of the tumor size data presented in (E).

Data in (D) and (F) represent mean \pm SEM (ANOVA with Tukey's multiple comparison test). * $p < 0.05$, ** $p < 0.001$, *** $p < 0.001$, **** $p < 0.0001$.

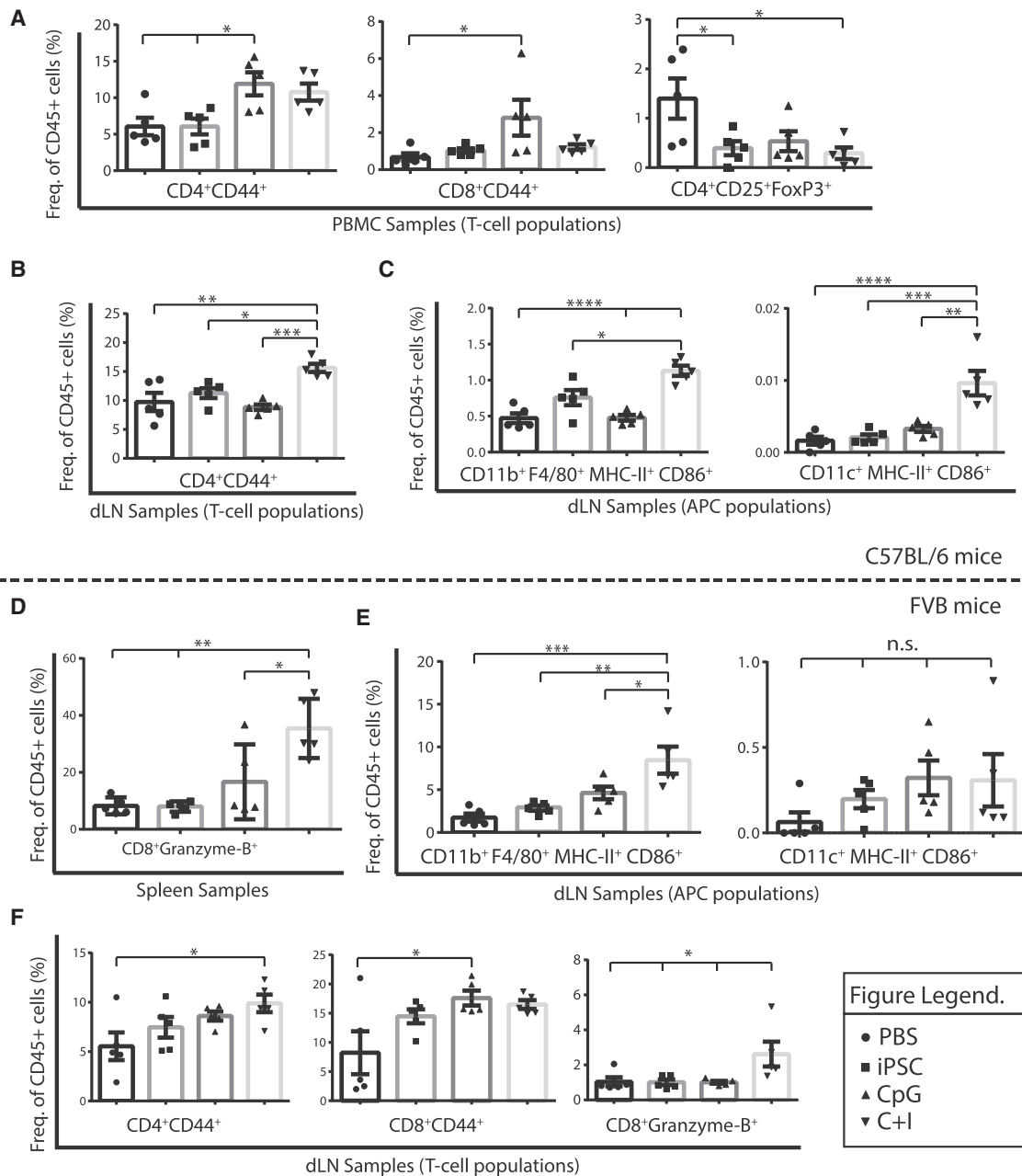


Figure 2. Prophylactic Vaccination Leads to Increased Antigen Presentation in dLNs and Subsequent Effector/Memory T Cell Responses in dLNs and Spleen

(A) 2 weeks after B16F0 introduction, iPSC- and C+I-vaccinated mice showed a significant reduction in percentages of regulatory T cells ($CD4^+CD25^+FoxP3^+$) and an increase in effector/memory helper T cells ($CD4^+CD44^+$) in the peripheral blood of C+I-vaccinated mice. At that point, only limited upregulation of effector/memory cytotoxic T cells ($CD8^+CD44^+$) was seen.

(B and C) The dLNs in the C+I group had significantly higher percentages of effector/memory helper T cells (B) and increased antigen presentation by mature antigen-presenting cells (APCs) such as macrophages ($CD11b^+F4/80^+MHC-II^+CD86^+$) and dendritic cells ($CD11c^+MHC-II^+CD86^+$) (C).

(D) C+I-vaccinated FVB mice showed increased percentages of activated cytotoxic T cells ($CD8^+Granzyme-B^+$) in spleens 4 weeks after DB7 introduction.

(E and F) dLNs of these mice revealed an increased frequency of mature antigen-presenting macrophages (E) as well as effector/memory helper T cells and cytotoxic T cells (F).

Data represent mean \pm SEM (n = 5 per group; ANOVA with Tukey's multiple comparison test). *p < 0.05, **p < 0.001, ***p < 0.001, ****p < 0.0001.

by demonstrating (1) cancer immunity by C+I primed T cells and (2) iPSC immunity by tumor-experienced lymphocytes (TEs). For the first experiment, isolated T cells from C+I-vaccinated or vehicle (PBS+CpG)-vaccinated mice were adoptively trans-

ferred to a group of tumor-bearing orthotopic breast cancer mice (n = 7 per group), and tumor growth was measured over the course of 4 weeks (Figure 4A). This resulted in a significant reduction of tumor sizes in the C+I-vaccinated group compared

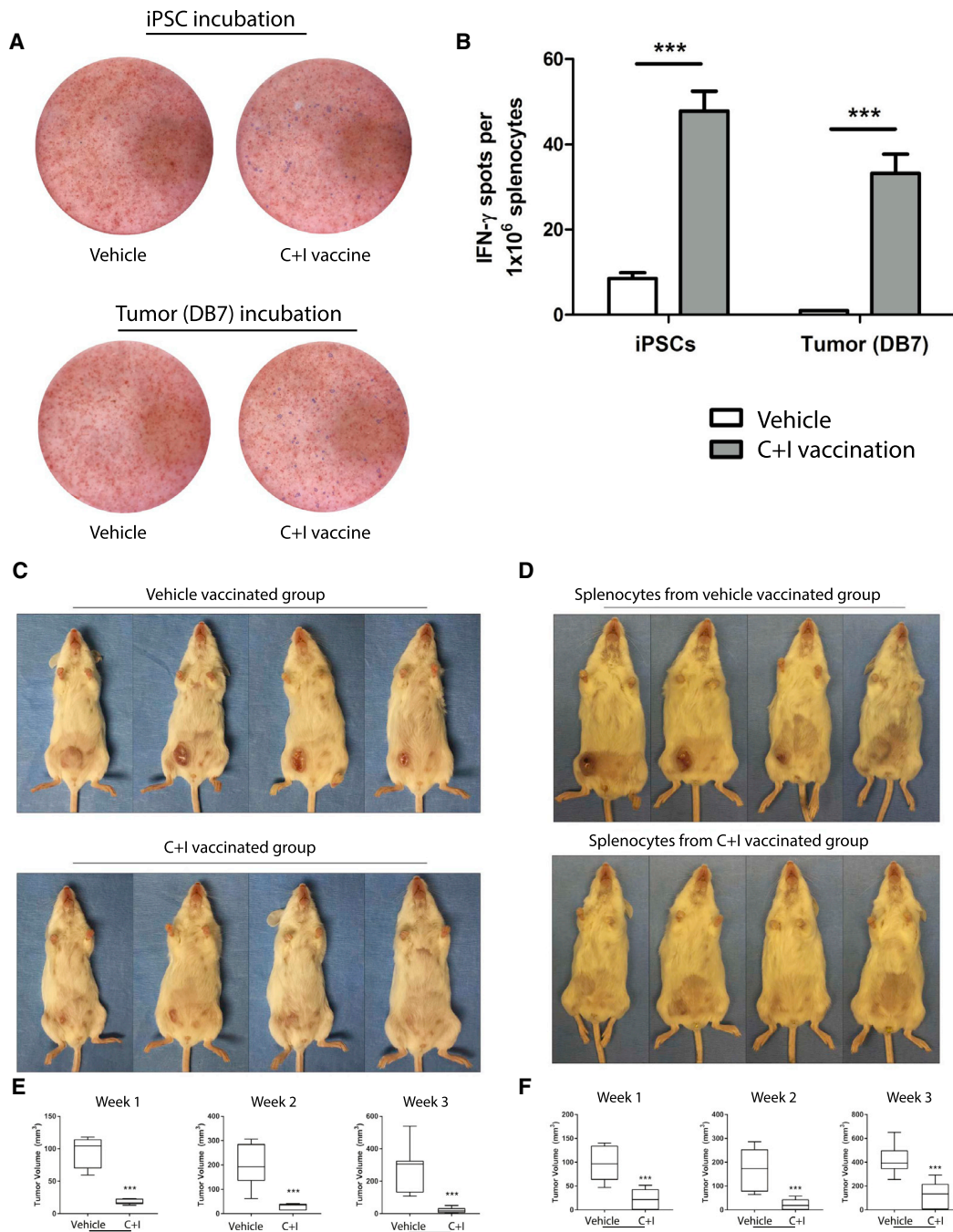


Figure 3. Tumor-Specific Properties of C+I Vaccine *In Vitro* and *In Vivo* in an Orthotopic Tumor Model of Breast Cancer

(A) Dual ELISpot assay (red, granzyme- β ; blue, IFN- γ) for immune cell activation of splenocytes in the C+I-vaccinated group (iPSC vaccinated; $n = 6$) compared to CpG alone (vehicle; $n = 4$) group upon exposure to iPSC lysate and DB7 lysate (see also [Figures S4A](#) and [S4B](#)).

(B) Significant increase of number of IFN- γ spots in the C+I-vaccinated group compared to the vehicle group. Spots were calculated using Adobe Photoshop software based on color differences. $***p < 0.001$ (Student's t test).

(C) Representative images of tumor volume in C+I-vaccinated mice compared to vehicle-vaccinated mice in an orthotopic tumor model of breast cancer 3 weeks after tumor inoculation.

(D) Representative images of tumor volume in tumor bearing mice after receiving adoptive transfer of splenocytes from C+I-vaccinated mice compared to vehicle-vaccinated mice in an orthotopic tumor model of breast cancer 3 weeks after adoptive transfer.

(E) Quantification of the results from (C) shows a significant reduction of tumor volume in C+I-vaccinated mice compared to vehicle-vaccinated mice in an orthotopic tumor model of breast cancer over the course of 3 weeks. $***p < 0.001$ (one way ANOVA).

(F) Significant reduction of tumor volume in tumor-bearing mice from (D) over the course of 3 weeks after adoptive transfer of splenocytes from C+I-vaccinated mice ($n = 7$) compared to mice receiving splenocytes from vehicle-vaccinated mice ($n = 8$). $***p < 0.001$ (one way ANOVA).

Mean \pm SEM.

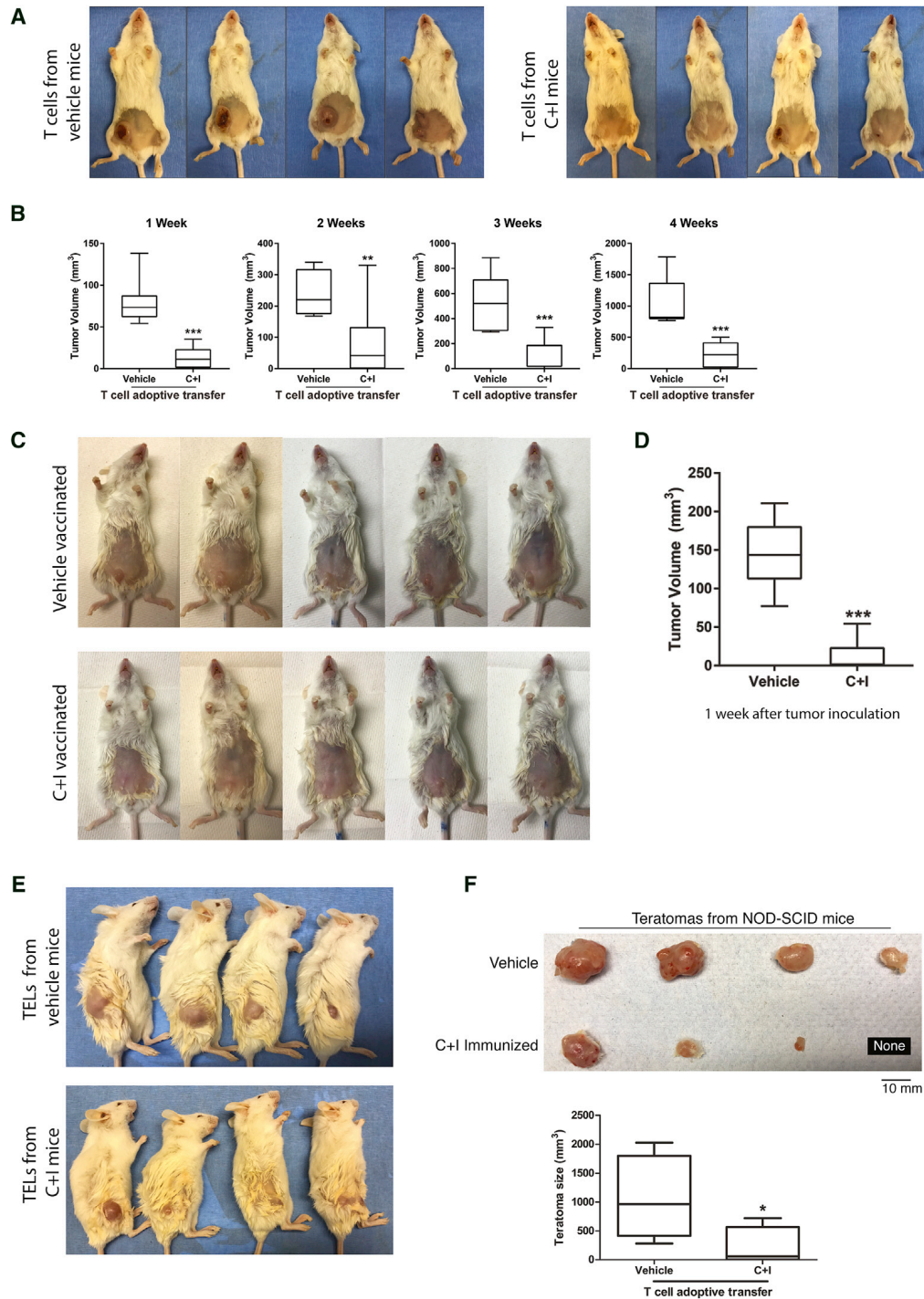


Figure 4. Shared Epitopes between Cancer Cells and iPSCs Provide T Cells with Two-Way Immunity

(A) Representative images from tumor-bearing mice 4 weeks after receiving T cells from either vehicle- or C+I-vaccinated mice.
 (B) Quantification of the tumor sizes of tumor-bearing mice in (A) over the course of 4 weeks after receiving T cells from vehicle- or C+I-vaccinated mice, as measured by caliper. Significant reduction of tumor sizes was seen as early as 1 week after the adoptive transfer of T cells from C+I-vaccinated mice and remained significantly reduced during the course of the experiment (**p < 0.01; ***p < 0.001; Student t test).
 (C) Representative images of vehicle (CpG only; n = 10) and C+I-vaccinated mice (n = 10) 1 week after orthotopic tumor inoculation.
 (D) Quantification of the tumor sizes displayed in (C) shows robust rejection of the DB7 breast cancer cells (***p < 0.001; Student t test).
 (E) Representative images of NOD-SCID mice receiving TELs from the dLNs from vehicle- or C+I-vaccinated mice from the experiment in (C) (n = 4 per group).
 (F) Images from the teratomas isolated from mice in (E, top). Quantification reveals a significant reduction in teratoma sizes (bottom) from the C+I-immunized group (*p < 0.05; Student t test).
 Mean ± SEM.

to the vehicle-vaccinated group as early as 1 week after the adoptive transfer (Figure 4B). For the second experiment, another batch of mice vaccinated with C+I (n = 10) or vehicle (n = 10) were inoculated with breast cancer cells, and tumor growth was measured at 1 week (Figures 4C and 4D). Afterward, we extracted TELs from the dLNs near the tumor site (Torcellan et al., 2017). These TELs were then adoptively transferred to iPSC-inoculated non-obese diabetic severe combined immunodeficiency (NOD-SCID) mice (5×10^6 TELs per mouse; n = 4 per group), and teratoma development was measured for 4 weeks. Significant reduction in teratoma sizes was seen at 4 weeks in the NOD-SCID mice receiving TELs from C+I animals that were able to reject the DB7 tumor cells, whereas mice receiving TELs from vehicle-vaccinated animals developed large teratomas (Figure 4E and 4F).

C+I Vaccination in a Mesothelioma Model Elicits a Pro-inflammatory Profile for Tumor-Infiltrating Lymphocytes

As an alternative model for prophylactic treatment, we selected the mesothelioma cell line AC29, syngeneic to CBA/J mice. Again, CBA/J iPSCs were created (Figures S2C and S2D), and mice were vaccinated for 4 weeks with PBS (P), CpG and iPSCs (C+I), or CpG with irradiated AC29 cancer cells (C+A) as a positive control. Afterward, 2×10^6 AC29 cells (A) or 2×10^6 iPSCs (I) were injected subcutaneously, and after 1 week, the TILs were analyzed for their immune profile and T cell receptor (TCR) sequences. Immune profiling was performed with cytometry by time-of-flight (CyTOF) analysis using a phenotype and intracellular staining kit, which revealed an increased presence of effector/memory CD4⁺ (24.0%) and CD8⁺ T cells (22.4%), with a reduction in T-regs in the C+I/A group (1.9%) compared to P/A control (21.1%, 14.2%, and 3.0%, respectively) (Figure 5A). Using Citrus (cluster identification, characterization, and regression) analysis (Bruggner et al., 2014), B cells and T cells expressing interleukin-2 (IL-2), IL-4, and IL-5 were found to be predictive of tumor regression in C+I-vaccinated mice compared to the PBS control group (Figures 5B, S5A, S5B, and S5D). Interestingly, systemic cytokine levels were significantly lower in the vaccinated group and were found to correlate with the positive control mice showing tumor rejection (C+I/iPSC; C+A/AC29) (Figures 6A, S6A, and S6B). TCR sequencing in the PBS control group revealed an overlap in T cell clones that are commonly present in thymus and spleen (Figure S6C). In contrast, the TCRs in the C+I group were more diverse among different mice. In addition, there was a generally lower frequency of the clones in the thymus and more similar frequencies in the spleen, likely because of mouse-specific responses to the C+I vaccine (Figures 6B and S6D). Interestingly, there was one TCR clone that was shared by four of five mice in the C+I group but was not present in any of the other groups; this clone was also extremely rare in naive mice.

C+I Adjuvant Therapy after Tumor Resection Leads to Decreased Tumor Load in Resection Areas and dLNs

To assess the effectiveness of the vaccine as an adjuvant therapy after tumor resection, we next injected 5×10^4 B16F0 tumor cells subcutaneously in the lower back of C57BL/6 mice and R2- or R1-resected mice after 2 weeks. R2-resected mice had no visible recurrence of melanoma in the resection area

(RA) after receiving two adjuvant rounds of C+I vaccine, whereas PBS-control-vaccinated mice had visible tumors within the RAs (Figure S7A). R1-resected mice were vaccinated for 4 weeks with the C+I vaccine (n = 10), CpG (n = 10), and PBS (n = 8) (Figure 7A), after which dLNs and RAs were analyzed using a tumor-specific primer designed to detect and quantify the B16F0 melanoma line (Figures S7B–S7G). Tumor load in the dLNs was reduced in both CpG-only and the C+I-vaccine groups, indicating that CpG acted as a potent adjuvant to induce tumor degradation upon near-tumor injection (Figure S7H). Interestingly, in areas more distant from the vaccination sites, only the C+I-vaccinated group had significantly lower tumor recurrence in the RA (Figure 7B). Systemically, this is explained by reactivation of the immune system (Chung et al., 2013; Dolcetti et al., 2010; Numasaki et al., 2003), as well as a reduction of B16 melanoma-promoting Th17 cells (He et al., 2010) compared to the control groups (Figures 7C, S5C, and S5E).

DISCUSSION

Tumor establishment and progression involve highly proliferative hypoinmunogenic cells that evade the surveillance of the immune system. Therefore, new avenues within the field of cancer treatment are being pursued to target cancer by reactivating the immune system. One way researchers are trying to achieve this is by using chimeric antigen receptors (CARs), with promising results (Lee et al., 2015; Maude et al., 2014; Maus et al., 2014). The idea behind this therapy is to create a cancer-specific antigen receptor and couple this to an effector cell (e.g., T cell), with newer generations of CARs that might even incorporate the co-stimulatory pathways. However, thus far, results have been mixed, with some patients relapsing, possibly due to loss of expression of the targeted antigen (Grupp et al., 2013; Maude et al., 2014). One way to circumvent this would be to identify new tumor-specific antigens, but large numbers of tumor antigens are still unknown.

Pluripotent cells and tissues share known and likely also unknown TSAs and TAAs with cancer cells and therefore could be a potential agent to prime an immune system to target cancer. This modified cell would then function as a surrogate cell type that resembles the targeted cancer type. A few groups have pursued the use of embryonic cells for priming the immune system in targeting cancer but thus far have not shown efficacy and safety for the treatment of various types of cancer (Li et al., 2009; Yaddanapudi et al., 2012). In addition, they still rely on the use of ethically concerning ESCs and a genetically modified cell line as an adjuvant (Yaddanapudi et al., 2012), making these treatments less suitable for personalized clinical translation.

In this study, we showed that prophylactic immunization of several mouse strains with an iPSC-based vaccine produces an effective immune response to multiple cancer types by upregulation of mature APCs in the dLNs with a subsequent increase in helper T cells and cytotoxic T cells locally and, later on, systemically. Interestingly, this led to a systemically favorable T-effector/T-reg ratio, which has been found to reduce tolerizing conditions (Zou, 2005). With our adoptive transfer data on transplantation of C+I-primed splenocytes into tumor-bearing mice, we demonstrated the tumor specificity of our iPSC vaccine, which, based on our *in vitro* data, was likely the result of

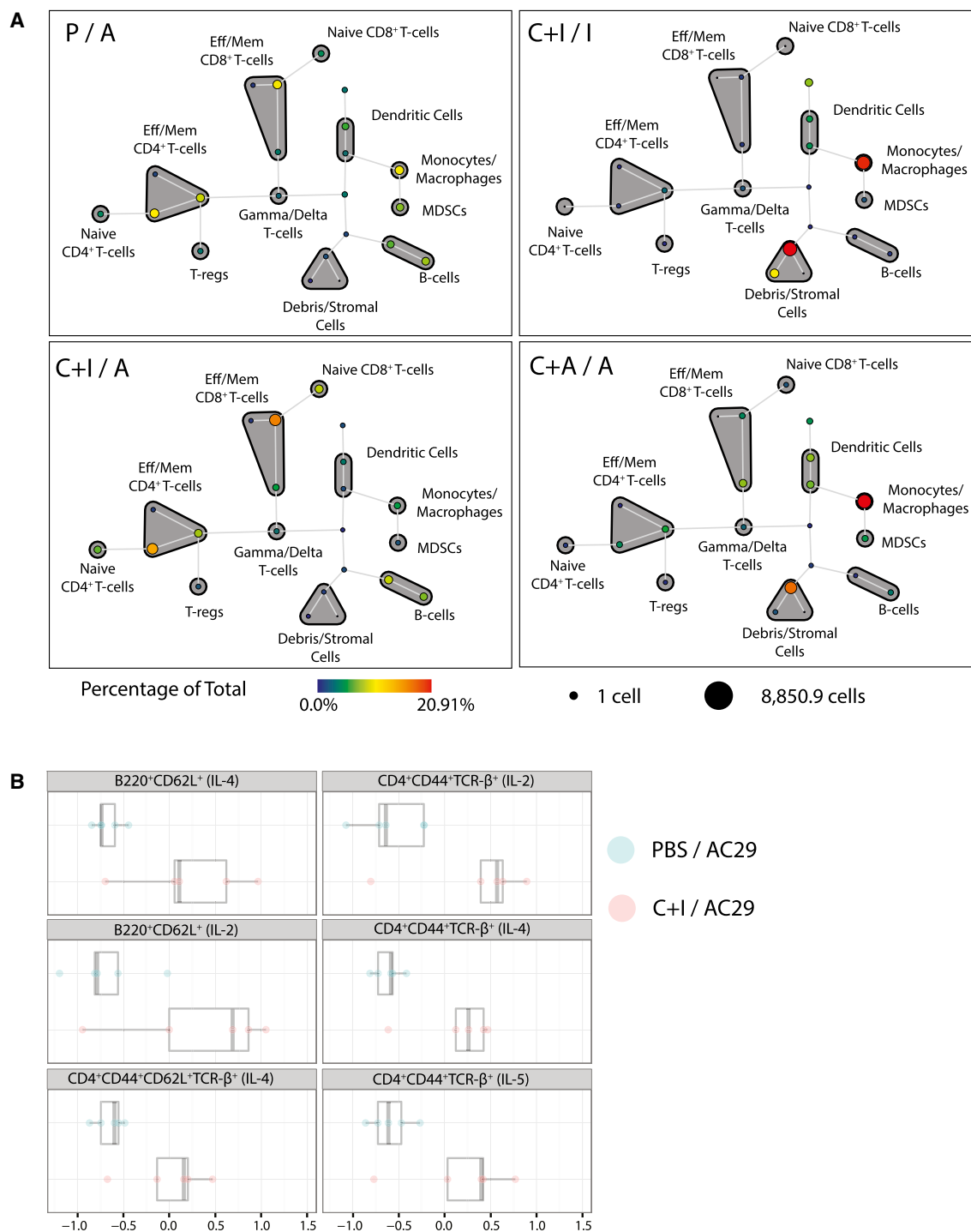


Figure 5. TILs Show a Pro-inflammatory Phenotype with B Cell and CD4⁺ T Cell Anti-tumor Responses

(A) 1 week after 2×10^6 AC29 (A) mesothelioma cells were injected in CpG+iPSC (C+I)-vaccinated mice ($n = 5$), TILs in this C+I/A group showed an increase in the frequency of effector/memory CD4⁺ and CD8⁺ cells and a reduction in T-reg numbers compared to PBS (P)-vaccinated mice ($n = 5$; P/A group), as assessed by spanning tree progression analysis of density-normalized events (SPADE) analysis of CyTOF data. The positive control groups, C+I-vaccinated and CpG+AC29 (C+A)-vaccinated mice, fully rejected iPSCs ($n = 5$; C+I/I) and AC29 cells ($n = 5$; C+A/A), respectively, with a subsequently enhanced presence of monocytes and macrophages and stromal cells.

(B) Citrus analysis of CyTOF data revealed that higher levels of IL-2, IL-4, and IL-5 in B cell and helper T cell clusters in the C+I mice are responsible for the intra-tumoral immune response.

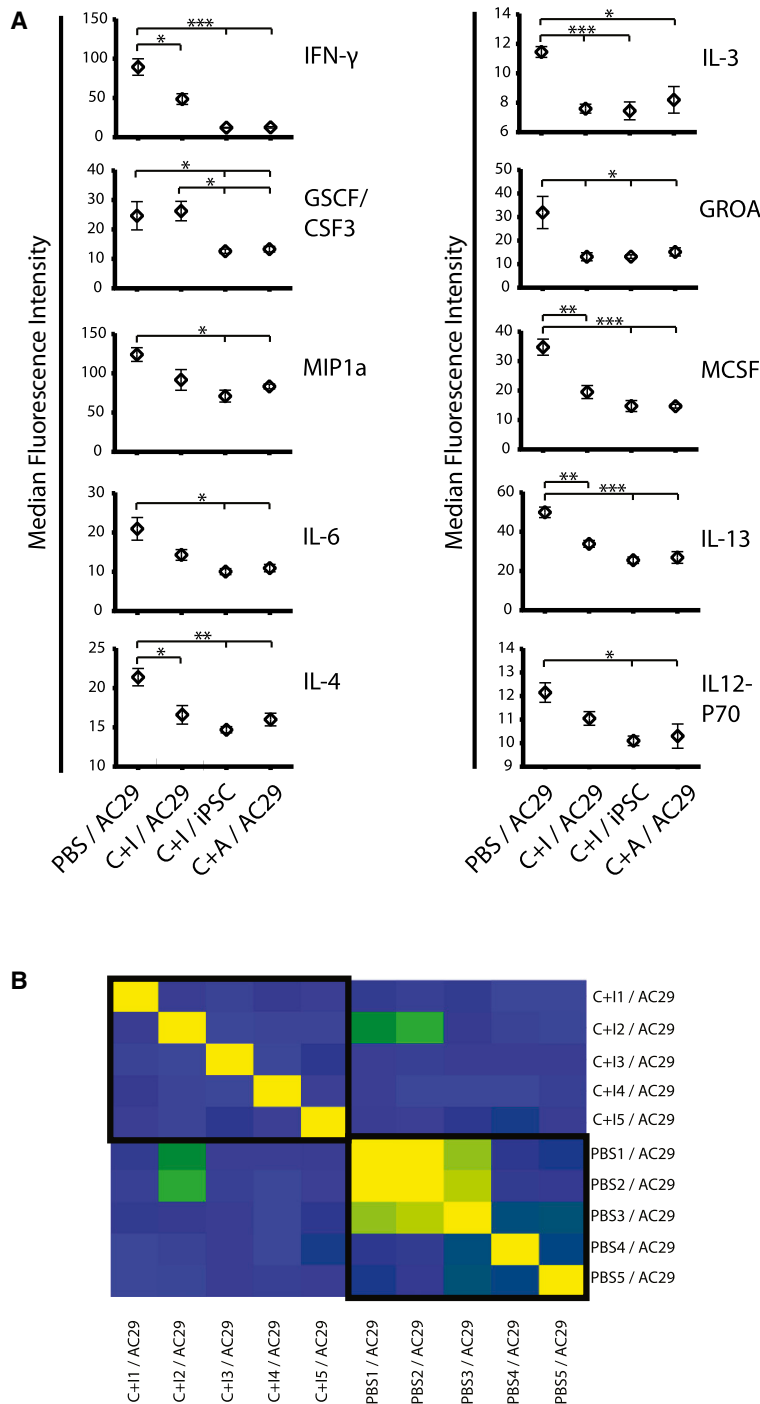


Figure 6. C+I Vaccination Leads to a Systemic Immune Profile Similar to Positive Control Groups of Tumor Rejection and Upregulation of Vaccine-Specific T Cell Clones

(A) Luminex analysis of serum from the different treatment groups 1 week after tumor cell introduction reveals a significantly lower presence of systemic cytokines in the positive control mice (C+I/iPSC, C+A/AC29) compared to PBS control mice (PBS/AC29). The C+I/AC29 group follows a similar trend as the positive control samples (C+I/iPSC and C+A/AC29; ANOVA with Tukey's multiple comparison test; * $p < 0.05$, ** $p < 0.001$, *** $p < 0.001$). (B) Among C+I-vaccinated mice (C+I1 through C+I5/AC29), there was greater unique vaccine-associated variance within the TILs, whereas PBS-vaccinated mice (PBS1 through 5/AC29) demonstrated a higher uniformity among T cells that are commonly present in lymphoid organs (Figures S6C and S6D). Mean \pm SEM.

we were able to show that C+I-primed T cells rejected the DB7 breast cancer cells and that the primed TELs were able to reduce teratoma size or stop teratoma formation altogether. This "two-way immunity" demonstrates shared epitopes between iPSCs and cancer cells.

Looking into the early intra-tumor immune response, we found mainly B cells and T cells expressing IL-2, IL-4, and IL-5 with a switch from common T cell clones to rarer vaccine-associated T cell clones. Most of these high-frequency clones vary between the vaccinated mice, suggesting that each mouse mounts a cross-reactive immune response based on different epitopes from the iPSCs. This provides further evidence that iPSCs share a larger repertoire of cancer-related epitopes, indicating that this surrogate cell type could be a potential candidate to limit the chances of immune evasion by the cancer cells as has occasionally reported in CAR therapy (Grupp et al., 2013; Maude et al., 2014).

IFN- γ ⁺ effector T cells. The lifespan of these IFN- γ ⁺ effector T cells (8–10 days) would also explain why there was tumor regression after the adoptive transfer of C+I-primed splenocytes in the orthotopic model of breast cancer for the first 2 weeks, after which a small increase in tumor size was seen (Dooms and Abbas, 2002). To test whether the immunity created by the vaccine is the result of shared epitopes between iPSCs and cancer cells, we performed adoptive transfer of C+I-primed T cells to breast-cancer-bearing mice and adoptive transfer of TELs to iPSC-inoculated NOD-SCID mice. With these experiments,

organ toxicity from cytokine storms upon transfusion of CAR T cells (Morgan et al., 2010). As we showed in our CBA/J mouse data using the Luminex assay, systemic cytokine levels are low; instead, there is a localized immune response within the tumor similar to the positive control group of tumor rejection. In addition, tissue analysis of our mice at different time points after vaccination did not show any increases in immune cells within heart and kidney tissues compared to negative control groups, nor were elevated levels of anti-nuclear antigen (ANA) IgG seen in serum from C+I-vaccinated mice.

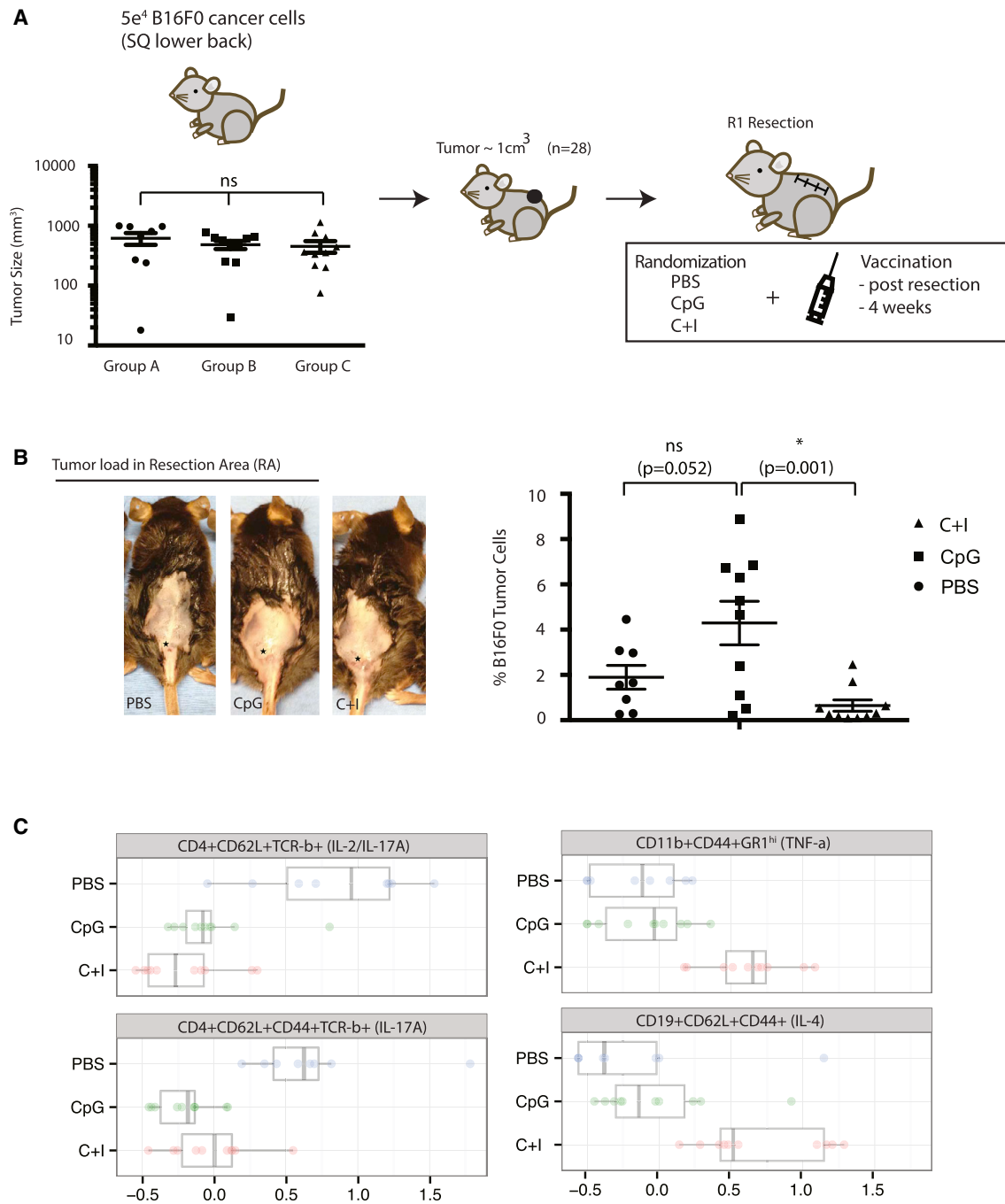


Figure 7. Adjuvant Vaccination after Tumor Resection Leads to Clean RAs and Reactivation of the Immune System to Target Cancer Cells

(A) B16F0 tumor-bearing mice underwent R1 tumor resection, were randomized into different treatment groups, and were vaccinated with C+I, CpG, or PBS for 4 weeks.

(B) DNA from skin biopsy specimens (*) in resection areas (RAs) showed a significant reduction in the percentage of tumor cells after four vaccination rounds with the C+I vaccine, as assessed by ddPCR.

(C) Vaccination post-tumor resection led to a reduction of Th17 cells (CD4⁺CD62L⁺TCR-b⁺(IL-2/IL-17A); CD4⁺CD62L⁺CD44⁺TCR-b⁺(IL-17A)) and an increased presence of TNF- α -expressing myeloid cells (CD11b⁺CD44⁺GR1^{hi}(TNF-a)) and IL-4-expressing CD19⁺CD62L⁺CD44⁺ B cells (n = 8 PBS, n = 10 CpG, n = 10 C+I; mean \pm SEM; ANOVA with Tukey's multiple comparison test; *p < 0.05). SQ, subcutaneous injection.

As a therapy for established melanomas, the C+I vaccine was not effective in reducing tumor growth, which is likely due to an established immunosuppressive tumor microenvironment that could potentially be remedied by combining the C+I vaccine with checkpoint blockade treatment (Le et al., 2015). However, as an adjuvant therapy after R1 resection of melanoma, we found that the C+I vaccine reactivated the immune system in rejecting remnant melanoma cells by the systemic upregulation of IL-4-expressing B cells and TNF- α -expressing CD11b⁺GR1^{hi} myeloid cells, as well as a reduction of tumor-promoting Th17 cells. In this setting, the cancer epitope heterogeneity of iPSCs, combined with the ease of their generation, may make this therapy readily available as adjuvant immunotherapy for multiple cancer types within weeks after diagnosis.

This last point is crucial for immunotherapy, because it is commonly known that the tumor microenvironment could limit effectiveness of tumor immunity by suppressive immune cells residing within the tumor. After debulking of the tumor and disrupting the tumor microenvironment to create an “inflamed” tumor site, immunotherapy should be more effective (Gajewski et al., 2013). This is demonstrated in our R1 resected melanoma model, which again emphasizes the need for a multi-TSA- and TAA-based vaccine to be readily available at time of tumor resection. Having a surrogate whole-cell vaccine with multiple known (and likely unknown) TSAs and TAAs available at such a short time after diagnosis would allow the priming of the immune system to target large numbers of cancer-specific antigens at a time when cancer cells are most vulnerable.

Even though an overlap was seen in murine and human TAA genes, it is important to note the differences in murine and human immunology before extrapolating the above-mentioned data to humans (Mestas and Hughes, 2004). Further testing of the C+I vaccine on human samples *ex vivo* should therefore be performed to show efficacy in humans.

Taken together, our data show the feasibility of creating broad tumor immunity against multiple cancer types using an iPSC-based vaccine that presents the immune system with large quantities of tumor antigens. Compared to current immunotherapy strategies, our iPSC vaccine is capable of reactivating the immune system to target established cancers without therapy-associated adverse effects and can be created within a few weeks after diagnosis. These beneficial properties make this iPSC vaccine a potential option for personalized adjuvant immunotherapy shortly after conventional primary treatment of cancer.

STAR★METHODS

Detailed methods are provided in the online version of this paper and include the following:

- KEY RESOURCES TABLE
- CONTACT FOR REAGENTS AND RESOURCE SHARING
- EXPERIMENTAL MODEL AND SUBJECT DETAILS
 - Animal models
 - Generation of murine iPSCs from fibroblasts
 - Cancer cell lines and implantation
- METHOD DETAILS
 - CpG + iPSC vaccine preparation and immunization
 - Mixed lymphocyte reaction (MLR)

- IgG binding assay
- Histopathology of explanted organs
- Isolation of inflammatory cells and serum from blood, spleen, tumor, and dLNs
- Staining of inflammatory cells for FACS analysis
- Teratoma formation
- Generation of tumor lysate
- Luminex multiplex cytokine assay
- ELISPOT assay
- Adoptive transfer of splenocytes and T cells
- Orthotopic tumor model
- Isolation of TELs from draining lymph nodes.
- Anti-nuclear antibody (ANA) ELISA
- Cytometry by Time of Flight (CyTOF)
- PCR detection of the large genomic deletion in Cdkn2a
- T cell Receptor (TCR) sequencing
- QUANTIFICATION AND STATISTICAL ANALYSES
 - Cluster identification, characterization and regression (Citrus)
 - Quantification of tumor load for melanoma by digital droplet PCR (ddPCR)
 - Analysis of RNA-sequencing data
 - Analysis of murine RNA sequencing data
- DATA AND SOFTWARE AVAILABILITY

SUPPLEMENTAL INFORMATION

Supplemental Information includes seven figures and can be found with this article online at <https://doi.org/10.1016/j.stem.2018.01.016>.

ACKNOWLEDGMENTS

We thank Dr. A. Connolly for the histopathology analysis of the hearts and kidneys, G. Busque for assistance with the caliper measurements of the tumors, and S. Carree and S. Limb for assistance with the graphic design of the cartoons. We also thank J. Churko for providing the RNA-sequencing data from the different human iPSC clones. This work was supported in part by Korean R&D grant HI14C3417 (Y.K.), California Institute of Regenerative Medicine (CIRM) grants DR2A-05394 and RT3-07798, and NIH grants R24 HL117756, R01 HL113006, R01 HL133272 (J.C.W.), and U19 AI057229 (M.M.D.).

AUTHOR CONTRIBUTIONS

N.G.K. developed the experimental design, performed and interpreted experiments, and wrote the manuscript. Y.K. performed and interpreted experiments. P.E.d.A. performed preliminary experiments and assisted with the experimental design. V.T. developed the digital droplet PCR (ddPCR) primers and performed the ddPCR. S.D. assisted with iPSC generation. N.-Y.S. performed biostatistical analyses on the RNA-sequencing data. T.-T.W. established the orthotopic breast cancer model and performed the adoptive transfer of splenocytes. H.Y. assisted with iPSC culture. D.D. assisted with the preliminary *in vitro* experiments. R.N. and T.P.B. assisted with the vaccinations, tumor measurements, harvest, and processing of tissues for downstream analyses. D.T.P. assisted with splenocyte isolation for adoptive transfer and analyzing the RNA-sequencing data. I.B. assisted with the optimization of the vaccination schedule. A.H. provided experimental advice with the T cell receptor sequencing. P.H.A.Q., J.F.H., R.L., and M.M.D. provided experimental advice and manuscript writing. J.C.W. provided experimental advice and design, manuscript writing, and funding support.

DECLARATION OF INTERESTS

The authors declare no competing interests.

Received: September 8, 2016
Revised: August 15, 2017
Accepted: January 19, 2018
Published: February 15, 2018

REFERENCES

- Anders, S., and Huber, W. (2010). Differential expression analysis for sequence count data. *Genome Biol.* **11**, R106.
- Anders, S., McCarthy, D.J., Chen, Y., Okoniewski, M., Smyth, G.K., Huber, W., and Robinson, M.D. (2013). Count-based differential expression analysis of RNA sequencing data using R and Bioconductor. *Nat. Protoc.* **8**, 1765–1786.
- Anders, S., Pyl, P.T., and Huber, W. (2015). HTSeq—a Python framework to work with high-throughput sequencing data. *Bioinformatics* **31**, 166–169.
- Ben-Porath, I., Thomson, M.W., Carey, V.J., Ge, R., Bell, G.W., Regev, A., and Weinberg, R.A. (2008). An embryonic stem cell-like gene expression signature in poorly differentiated aggressive human tumors. *Nat. Genet.* **40**, 499–507.
- Bock, C., Kiskinis, E., Verstappen, G., Gu, H., Boulting, G., Smith, Z.D., Ziller, M., Croft, G.F., Amoroso, M.W., Oakley, D.H., et al. (2011). Reference Maps of human ES and iPSC cell variation enable high-throughput characterization of pluripotent cell lines. *Cell* **144**, 439–452.
- Brewer, B.G., Mitchell, R.A., Harandi, A., and Eaton, J.W. (2009). Embryonic vaccines against cancer: an early history. *Exp. Mol. Pathol.* **86**, 192–197.
- Bruggner, R.V., Bodenmiller, B., Dill, D.L., Tibshirani, R.J., and Nolan, G.P. (2014). Automated identification of stratifying signatures in cellular subpopulations. *Proc. Natl. Acad. Sci. USA* **111**, E2770–E2777.
- Chang, G., Gao, S., Hou, X., Xu, Z., Liu, Y., Kang, L., Tao, Y., Liu, W., Huang, B., Kou, X., et al. (2014). High-throughput sequencing reveals the disruption of methylation of imprinted gene in induced pluripotent stem cells. *Cell Res.* **24**, 293–306.
- Chen, J.Y., Tang, Y.A., Huang, S.M., Juan, H.F., Wu, L.W., Sun, Y.C., Wang, S.C., Wu, K.W., Balraj, G., Chang, T.T., et al. (2011). A novel sialyltransferase inhibitor suppresses FAK/paxillin signaling and cancer angiogenesis and metastasis pathways. *Cancer Res.* **71**, 473–483.
- Chung, A.S., Wu, X., Zhuang, G., Ngu, H., Kasman, I., Zhang, J., Vernes, J.M., Jiang, Z., Meng, Y.G., Peale, F.V., et al. (2013). An interleukin-17-mediated paracrine network promotes tumor resistance to anti-angiogenic therapy. *Nat. Med.* **19**, 1114–1123.
- Churko, J., Lee, J., Ameen, M., Gu, M., Venkaasubramanian, M., Diecke, S., Sallam, K., Im, H., Wang, G., Gold, J.D., et al. (2017). Transcriptomic and epigenomic differences in human induced pluripotent stem cells generated from six reprogramming methods. *Nat. Biomed. Eng.* **1**, 826–837.
- Consortium, E.P.; ENCODE Project Consortium (2011). A user's guide to the encyclopedia of DNA elements (ENCODE). *PLoS Biol.* **9**, e1001046.
- de Almeida, P.E., Meyer, E.H., Kooreman, N.G., Diecke, S., Dey, D., Sanchez-Freire, V., Hu, S., Ebert, A., Odegaard, J., Mordwinkin, N.M., et al. (2014). Transplanted terminally differentiated induced pluripotent stem cells are accepted by immune mechanisms similar to self-tolerance. *Nat. Commun.* **5**, 3903.
- Diecke, S., Lu, J., Lee, J., Termglinchan, V., Kooreman, N.G., Burrridge, P.W., Ebert, A.D., Churko, J.M., Sharma, A., Kay, M.A., and Wu, J.C. (2015). Novel codon-optimized mini-intronic plasmid for efficient, inexpensive, and xeno-free induction of pluripotency. *Sci. Rep.* **5**, 8081.
- Dolcetti, L., Peranzoni, E., Ugel, S., Marigo, I., Fernandez Gomez, A., Mesa, C., Geilich, M., Winkels, G., Traggiai, E., Casati, A., et al. (2010). Hierarchy of immunosuppressive strength among myeloid-derived suppressor cell subsets is determined by GM-CSF. *Eur. J. Immunol.* **40**, 22–35.
- Dooms, H., and Abbas, A.K. (2002). Life and death in effector T cells. *Nat. Immunol.* **3**, 797–798.
- Evans, M.S., Chaurette, J.P., Adams, S.T., Jr., Reddy, G.R., Paley, M.A., Aronin, N., Prescher, J.A., and Miller, S.C. (2014). A synthetic luciferin improves bioluminescence imaging in live mice. *Nat. Methods* **11**, 393–395.
- Gajewski, T.F., Schreiber, H., and Fu, Y.X. (2013). Innate and adaptive immune cells in the tumor microenvironment. *Nat. Immunol.* **14**, 1014–1022.
- Galvan, D.L., O'Neil, R.T., Foster, A.E., Huye, L., Bear, A., Rooney, C.M., and Wilson, M.H. (2015). Anti-tumor effects after adoptive transfer of IL-12 transposon-modified murine splenocytes in the OT-I-melanoma mouse Model. *PLoS ONE* **10**, e0140744.
- Ghosh, Z., Huang, M., Hu, S., Wilson, K.D., Dey, D., and Wu, J.C. (2011). Dissecting the oncogenic and tumorigenic potential of differentiated human induced pluripotent stem cells and human embryonic stem cells. *Cancer Res.* **71**, 5030–5039.
- Gilkeson, G.S., Conover, J., Halpern, M., Pissetsky, D.S., Feagin, A., and Klinman, D.M. (1998). Effects of bacterial DNA on cytokine production by (NZB/NZW)F1 mice. *J. Immunol.* **161**, 3890–3895.
- Goldstein, M.J., Varghese, B., Brody, J.D., Rajapaksa, R., Kohrt, H., Czerwinski, D.K., Levy, S., and Levy, R. (2011). A CpG-loaded tumor cell vaccine induces antitumor CD4+ T cells that are effective in adoptive therapy for large and established tumors. *Blood* **117**, 118–127.
- Grupp, S.A., Kalos, M., Barrett, D., Aplenc, R., Porter, D.L., Rheingold, S.R., Teachey, D.T., Chew, A., Hauck, B., Wright, J.F., et al. (2013). Chimeric antigen receptor-modified T cells for acute lymphoid leukemia. *N. Engl. J. Med.* **368**, 1509–1518.
- Harrow, J., Frankish, A., Gonzalez, J.M., Tapanari, E., Diekhans, M., Kokocinski, F., Aken, B.L., Barrell, D., Zadissa, A., Searle, S., et al. (2012). GENCODE: the reference human genome annotation for The ENCODE Project. *Genome Res.* **22**, 1760–1774.
- He, D., Li, H., Yusuf, N., Elmets, C.A., Li, J., Mountz, J.D., and Xu, H. (2010). IL-17 promotes tumor development through the induction of tumor promoting microenvironments at tumor sites and myeloid-derived suppressor cells. *J. Immunol.* **184**, 2281–2288.
- Kim, D., Langmead, B., and Salzberg, S.L. (2015). HISAT: a fast spliced aligner with low memory requirements. *Nat. Methods* **12**, 357–360.
- Kocatürk, B., and Versteeg, H.H. (2015). Orthotopic injection of breast cancer cells into the mammary fat pad of mice to study tumor growth. *J. Vis. Exp.* **96**, 51967.
- Kooreman, N.G., and Wu, J.C. (2010). Tumorigenicity of pluripotent stem cells: biological insights from molecular imaging. *J. R. Soc. Interface* **7** (Suppl 6), S753–S763.
- Le, D.T., Uram, J.N., Wang, H., Bartlett, B.R., Kemberling, H., Eyring, A.D., Skora, A.D., Luber, B.S., Azad, N.S., Laheru, D., et al. (2015). PD-1 blockade in tumors with mismatch-repair deficiency. *N. Engl. J. Med.* **372**, 2509–2520.
- Lee, A.S., Tang, C., Rao, M.S., Weissman, I.L., and Wu, J.C. (2013). Tumorigenicity as a clinical hurdle for pluripotent stem cell therapies. *Nat. Med.* **19**, 998–1004.
- Lee, D.W., Kochenderfer, J.N., Stetler-Stevenson, M., Cui, Y.K., Delbrook, C., Feldman, S.A., Fry, T.J., Orentas, R., Sabatino, M., Shah, N.N., et al. (2015). T cells expressing CD19 chimeric antigen receptors for acute lymphoblastic leukaemia in children and young adults: a phase 1 dose-escalation trial. *Lancet* **385**, 517–528.
- Li, Y., Zeng, H., Xu, R.H., Liu, B., and Li, Z. (2009). Vaccination with human pluripotent stem cells generates a broad spectrum of immunological and clinical responses against colon cancer. *Stem Cells* **27**, 3103–3111.
- Mallon, B.S., Chenoweth, J.G., Johnson, K.R., Hamilton, R.S., Tesar, P.J., Yavatkar, A.S., Tyson, L.J., Park, K., Chen, K.G., Fann, Y.C., and McKay, R.D. (2013). StemCellDB: the human pluripotent stem cell database at the National Institutes of Health. *Stem Cell Res. (Amst.)* **10**, 57–66.
- Mallon, B.S., Hamilton, R.S., Kozhich, O.A., Johnson, K.R., Fann, Y.C., Rao, M.S., and Robey, P.G. (2014). Comparison of the molecular profiles of human embryonic and induced pluripotent stem cells of isogenic origin. *Stem Cell Res. (Amst.)* **12**, 376–386.
- Maude, S.L., Frey, N., Shaw, P.A., Aplenc, R., Barrett, D.M., Bunin, N.J., Chew, A., Gonzalez, V.E., Zheng, Z., Lacey, S.F., et al. (2014). Chimeric antigen receptor T cells for sustained remissions in leukemia. *N. Engl. J. Med.* **371**, 1507–1517.
- Maus, M.V., Grupp, S.A., Porter, D.L., and June, C.H. (2014). Antibody-modified T cells: CARs take the front seat for hematologic malignancies. *Blood* **123**, 2625–2635.

- Mestas, J., and Hughes, C.C. (2004). Of mice and not men: differences between mouse and human immunology. *J. Immunol.* *172*, 2731–2738.
- Mor, G., Singla, M., Steinberg, A.D., Hoffman, S.L., Okuda, K., and Klinman, D.M. (1997). Do DNA vaccines induce autoimmune disease? *Hum. Gene Ther.* *8*, 293–300.
- Morgan, R.A., Yang, J.C., Kitano, M., Dudley, M.E., Laurencot, C.M., and Rosenberg, S.A. (2010). Case report of a serious adverse event following the administration of T cells transduced with a chimeric antigen receptor recognizing ERBB2. *Mol. Ther.* *18*, 843–851.
- Mukherjee, P., Pathangey, L.B., Bradley, J.B., Tinder, T.L., Basu, G.D., Akporiaye, E.T., and Gendler, S.J. (2007). MUC1-specific immune therapy generates a strong anti-tumor response in a MUC1-tolerant colon cancer model. *Vaccine* *25*, 1607–1618.
- Naas, T., Ghorbani, M., Soare, C., Scherling, N., Muller, R., Ghorbani, P., and Diaz-Mitoma, F. (2010). Adoptive transfer of splenocytes to study cell-mediated immune responses in hepatitis C infection using HCV transgenic mice. *Comp. Hepatol.* *9*, 7.
- Nelakanti, R.V., Kooreman, N.G., and Wu, J.C. (2015). Teratoma formation: a tool for monitoring pluripotency in stem cell research. *Curr. Protoc. Stem Cell Biol.* *32*, 4A.8.1–4A.8.17.
- Numasaki, M., Fukushi, J., Ono, M., Narula, S.K., Zavodny, P.J., Kudo, T., Robbins, P.D., Tahara, H., and Lotze, M.T. (2003). Interleukin-17 promotes angiogenesis and tumor growth. *Blood* *101*, 2620–2627.
- Palena, C., Abrams, S.I., Schlom, J., and Hodge, J.W. (2006). Cancer vaccines: preclinical studies and novel strategies. *Adv. Cancer Res.* *95*, 115–145.
- Qiu, P., Simonds, E.F., Bendall, S.C., Gibbs, K.D., Jr., Bruggner, R.V., Linderman, M.D., Sachs, K., Nolan, G.P., and Plevritis, S.K. (2011). Extracting a cellular hierarchy from high-dimensional cytometry data with SPADE. *Nat. Biotechnol.* *29*, 886–891.
- Sodhi, A., Tandon, P., and Sarna, S. (1985). Adoptive transfer of immunity against solid fibrosarcoma in mice with splenocytes and peritoneal exudate cells obtained after in vitro sensitization and in vivo immunization with cis-dichlorodiamine platinum(II) treated fibrosarcoma cells. *Arch. Geschwulstforsch.* *55*, 47–61.
- Soldner, F., Hockemeyer, D., Beard, C., Gao, Q., Bell, G.W., Cook, E.G., Hargus, G., Blak, A., Cooper, O., Mitalipova, M., et al. (2009). Parkinson's disease patient-derived induced pluripotent stem cells free of viral reprogramming factors. *Cell* *136*, 964–977.
- Takahashi, K., and Yamanaka, S. (2006). Induction of pluripotent stem cells from mouse embryonic and adult fibroblast cultures by defined factors. *Cell* *126*, 663–676.
- Takahashi, K., Tanabe, K., Ohnuki, M., Narita, M., Ichisaka, T., Tomoda, K., and Yamanaka, S. (2007). Induction of pluripotent stem cells from adult human fibroblasts by defined factors. *Cell* *131*, 861–872.
- Torcellan, T., Hampton, H.R., Bailey, J., Tomura, M., Brink, R., and Chtanova, T. (2017). In vivo photolabeling of tumor-infiltrating cells reveals highly regulated egress of T-cell subsets from tumors. *Proc. Natl. Acad. Sci. USA* *114*, 5677–5682.
- Yaddanapudi, K., Mitchell, R.A., Putty, K., Willer, S., Sharma, R.K., Yan, J., Bodduluri, H., and Eaton, J.W. (2012). Vaccination with embryonic stem cells protects against lung cancer: is a broad-spectrum prophylactic vaccine against cancer possible? *PLoS ONE* *7*, e42289.
- Zhao, T., Zhang, Z.N., Rong, Z., and Xu, Y. (2011). Immunogenicity of induced pluripotent stem cells. *Nature* *474*, 212–215.
- Zou, W. (2005). Immunosuppressive networks in the tumour environment and their therapeutic relevance. *Nat. Rev. Cancer* *5*, 263–274.

STAR★METHODS

KEY RESOURCES TABLE

REAGENT or RESOURCE	SOURCE	IDENTIFIER
Antibodies		
PE/Cy7 anti-mouse CD3	eBioscience	25-0031-82; RRID: AB_469572
APC anti-mouse CD4	BD Bioscience	553051
PE anti-mouse CD4	eBioscience	12-0042-83; RRID: AB_465510
PerCP/Cy5.5 anti-mouse CD8	Biolegend	100734; RRID: AB_2075238
PE/Cy7 anti-mouse CD11b	Biolegend	101216; RRID: AB_312799
Pacific Blue anti-mouse/human CD44	Biolegend	103020; RRID: AB_493683
APC anti-mouse CD11c	Biolegend	117310; RRID: AB_313779
FITC anti-mouse CD86	BD Bioscience	553691
eFluor 450 anti-mouse F4/80	eBioscience	48-4801-82; RRID: AB_1548747
Alexa Fluor 488 anti-mouse FoxP3	Biolegend	126406; RRID: AB_1089113
PE anti-mouse Granzyme-B	eBioscience	12-8898-82; RRID: AB_10870787
Brilliant Violet 510 anti-mouse CD45	eBioscience	103137; RRID: AB_2561392
Alexa Fluor 700 anti-mouse CD25	eBioscience	56-0251-82; RRID: AB_891422
eFluor 780 Fixable Viability Dye	eBioscience	65-0865-14
Alexa Fluor 700 anti-mouse GR-1 Ly6	Biolegend	108422; RRID: AB_2137487
PerCP/Cy5.5 anti-mouse NK1.1	Biolegend	108728; RRID: AB_2132705
PerCP/Cy5.5 anti-mouse DX-5	Biolegend	108916; RRID: AB_2129358
PE anti-mouse MHC-II	eBioscience	12-5321-81; RRID: AB_465928
Alexa Fluor 488 anti-mouse IgG	Thermo Fisher Scientific	A-11001; RRID: AB_2534069
Anti-rabbit IgG Cross-adsorbed	Thermo Fisher Scientific	31213; RRID: AB_228376
Pacific Blue Rat IgG2b κ isotype control	Biolegend	400627
Alexa Fluor 488 Rat IgG2b κ isotype control	Biolegend	400625
PE Rat IgG2b κ isotype control	Thermo-Fisher Scientific	12-4031-82; RRID: AB_470042
FITC Rat IgG2a κ isotype control	BD Biosciences	553929
PE Rat IgG2a κ isotype control	eBioscience	12-4321-80; RRID: AB_1834380
Alexa Fluor 700 Rat IgG1 κ isotype control	eBioscience	56-4301-80; RRID: AB_494017
Anti SSEA-1 microbeads	Miltenyi Biotec	130-094-530
Oct 3/4 anti-mouse	Santa Cruz Biotechnology	sc-5279
c-Myc anti-mouse	EMD Millipore	06-340
SSEA-1 anti-mouse	EMD Millipore	MAB4301
Nanog anti-mouse	Santa Cruz Biotechnology	sc-33760
Sox2 anti-mouse	Santa Cruz Biotechnology	sc-365823
Mouse on Mouse (M.O.M.) Basic Kit	Vector Laboratories	BMK-2202
Fc Block anti-mouse	BD Biosciences	553141
Chemicals, Peptides, and Recombinant Proteins		
DMEM, high glucose, GlutaMAX	GIBCO	10569-010
Fetal Bovine Serum	Life Technologies	26140079
DPBS, no calcium, no magnesium	GIBCO	14190250
MEM Non-Essential Amino Acids	GIBCO	11140050
TrypLE Express	GIBCO	12605-036
CpG ODN 1826	Invivogen	tlrl-1826-1
Murine Leukemia Inhibitory Factor (mLIF)	EMD Millipore	ESG1106
Gelatin	Sigma Aldrich	G1393-100ML
Isothesia	Henry Schein	029405

(Continued on next page)

Continued

REAGENT or RESOURCE	SOURCE	IDENTIFIER
Matrigel matrix growth factor reduced	BD Biosciences	356231
RPMI medium 1640	Life Technologies	11875-119
ACK lysis buffer	Quality Biological	118-156-101
Collagenase D	Roche	11088882001
Deoxyribonuclease I from bovine pancreas	Sigma Aldrich	D4263-5VL
Trypsin Inhibitor	Sigma Aldrich	T9003-1G
HEPES 1M	Sigma Aldrich	H3662
Percoll GE Density Gradient Media	VWR	89428-524
UltraPure 0.5M EDTA	Life Technologies	15575-020
PrimeStar GXL DNA Polymerase	Clontech	R050A
ddPCR Supermix for Probes	Bio-Rad	1863024
Critical Commercial Assays		
Neon Transfection System 100 μ l Kit	Thermo Fisher Scientific	MPK10025
MycAlert Detection Kit	Lonza	LT07-318
MycAlert Assay Control Set	Lonza	LT07-518
CFSE Cell Trace staining	Thermo Fisher Scientific	C34554
Mouse Th1/Th2/Th17 Cytokine Multi-Analyte ELISArray	QIAGEN	MEM-003A
MaxPar Mouse Spleen/Lymph Node Phenotyping kit	Fluidigm	201306
MaxPar Mouse Intracellular Cytokine I Panel kit	Fluidigm	201310
Cisplatin viability dye	Fluidigm	201062
Cytofix/Cytoperm Permeabilization Solution kit	BD Biosciences	BDB554714
Pierce BCA Protein Assay Kit	Thermo Fisher Scientific	23225
Mouse IFN- γ /Granzyme B Dual-Color ELISpot Kit	R&D Systems	ELD5819
Pan T cell Isolation Kit II, mouse	Miltenyi Biotec	130-095-130
Anti-nuclear Antigen (IgG) mouse ELISA Kit	Antibodies-Online	ABIN366290
DNeasy Blood & Tissue kit	QIAGEN	69504
Deposited Data		
TCR β sequencing tumor-infiltrating lymphocytes	This paper	immunoACCESS: DOI: 10.21417/B7B648
RNA-seq from human somatic/cancer cell lines	ENCODE project	https://www.genome.gov/encode/
RNA-seq from human iPSC cells	Churko et al., 2017	N/A
RNA-seq from murine somatic cell lines	ENCODE project	http://mouseencode.org/
RNA-seq from murine iPSC cells	Chang et al., 2014	N/A
Experimental Models: Cell Lines		
EmbryoMax Primary Mouse Embryo Fibroblasts	EMD Millipore	PMEF-N
DB7 breast cancer cells	The University of Utah; Dr. Joe Smith	N/A
B16F0 melanoma cells	ATCC	CRL-6322
AC29 mesothelioma cells	Sigma Aldrich	10092308
Experimental Models: Organisms/Strains		
Mouse: FVB/NJ	The Jackson Laboratory	001800
Mouse: C57BL/6J	The Jackson Laboratory	000664
Mouse: CBA/J	The Jackson Laboratory	000656
NOD-SCID IL2R γ ^{null} (NSG)	The Jackson Laboratory	005557
Oligonucleotides		
TaqMan Copy Number TFRC probe (Mm00000692_cn)	Thermo Fisher Scientific	4400291
5'ACTAGCCAGAGGATCTTAAGACT3'	This paper	N/A
5'GCCATCACTGGAAAGAGAGGC3'	This paper	N/A
5'(HEX)CCTGCCCCACCCACTCCCCCTTTT (Blackhole Quencher)3'	This paper	N/A

(Continued on next page)

Continued

REAGENT or RESOURCE	SOURCE	IDENTIFIER
Recombinant DNA		
Codon-optimized mini-intronic plasmid (coMIP)	Diecke et al., 2015	N/A
Software and Algorithms		
ImmunoSeq Analyzer	Adaptive Biotechnologies	http://clients.adaptivebiotech.com/
Prism GraphPad 7	GraphPad Software	https://www.graphpad.com/scientific-software/prism/
Cytobank	Cytobank	https://stanford.cytobank.org/cytobank/login
Citrus 0.8	Nolan lab; Stanford, USA.	https://github.com/nolanlab/citrus/wiki/Installing-Citrus
R; version 3.0.3	The R Project	https://www.r-project.org/
Adobe Photoshop CS6	Adobe	http://www.adobe.com/nl/products/photoshop.html
Other		
29 Gauge x +1/2" needle 3/10cc	Terumo Medical	SS30M2913
Multiplex-Luminex platform (LabMap200 System)	HIMC; Stanford University, USA	N/A

CONTACT FOR REAGENTS AND RESOURCE SHARING

Further information and requests for resources and reagents should be directed to and will be fulfilled by the Lead Contact, Joseph C. Wu (joewu@stanford.edu).

EXPERIMENTAL MODEL AND SUBJECT DETAILS

Animal models

Young adult female FVB, C57BL/6J, and CBA/J mice (6-8 weeks old) were used. Animals were randomly assigned to the different treatment groups. Tumor-bearing mice were excluded from the experiment if their physical condition required euthanasia before the experimental deadline, due to criteria such as tumor sizes exceeding 1 cm³, visible distress, pain, or illness. All experiments were approved by the Stanford University Administrative Panel of Laboratory Animal Care (APLAC).

Generation of murine iPSCs from fibroblasts

Fibroblasts from FVB, C57BL/6J, and CBA/J mice (The Jackson Laboratory, Bar Harbor, Maine) were grown in DMEM Glutamax (ThermoFisher Scientific, Waltham, MA, USA) with 20% fetal bovine serum (FBS) and 1x NEAA (ThermoFisher Scientific). Fibroblasts were dissociated using TrypLE Express (ThermoFisher Scientific) and 1x10⁶ fibroblasts were resuspended in electroporation buffer (Neon system, ThermoFisher Scientific). Cells were transfected with a codon-optimized mini-intronic plasmid (coMIP) containing the four reprogramming factors *Oct-4*, *Sox-2*, *c-Myc*, and *Klf4* (Diecke et al., 2015). After transfection, cells were plated on irradiated mouse embryonic feeder (MEF) cells and cultured in DMEM with 15% FBS, 1x NEAA, and 10 ng/ml murine leukemia inhibiting factor (mLIF; EMD Millipore, MA, USA). After iPSC colonies started to appear, they were manually picked and transferred to a fresh feeder layer. The iPSC colonies were grown for a few passages and then transferred to 0.2% gelatin-coated plates to be sorted for SSEA-1 using magnetic bead sorting (Miltenyi, Germany) to keep a pure undifferentiated population. For characterization, iPSCs were stained for Oct4, Nanog, Sox2 (Santa Cruz, CA, USA), SSEA1, and c-Myc (EMD Millipore) to assess pluripotency. In addition, a teratoma assay was performed on all iPSC lines by transplantation of 1x10⁶ iPSCs in the hindlimb of NOD-SCID mice (The Jackson Laboratory). All cell lines were tested for mycoplasma contamination and found to be negative.

Cancer cell lines and implantation

The breast cancer line DB7 was a gift from Dr. Joe Smith (University of Utah, USA). It was derived from FVB mice and is a non-metastatic cell line. The B16F0 melanoma cell line was purchased from ATCC (Manassas, VA, USA) and is syngeneic to C57BL/6 mice. It has low-grade lymphoid metastatic potential to the lungs. The AC29 mesothelioma cancer line was purchased from Sigma-Aldrich (St. Louis, MO, USA). The cancer lines were grown in DMEM, 10% FBS under normal culture conditions. For the C57BL/6 and FVB mice, 5x10⁴ cancer cells were resuspended in 100 μL PBS and injected subcutaneously in the lower back of the mice. The CBA/J mice were injected with 2x10⁶ cancer cells. Tumor growth was assessed weekly by caliper measurement. At the end of the study, tumors were explanted and gross examination of draining lymph nodes and lung tissue was performed for any metastases.

METHOD DETAILS

CpG + iPSC vaccine preparation and immunization

For each mouse, 2×10^6 SSEA-1-sorted syngeneic murine iPSCs were irradiated at 6,000 rads prior to injection. Cells were suspended in 100 μ L of 5 μ M CpG (Invivogen, San Diego, USA), dissolved in PBS, and loaded into 1/4 cc insulin syringes (Terumo). Mice were placed in an induction chamber and anesthetized with 2% isoflurane (Isothesia, Butler Schein) in 100% oxygen with a delivery rate of 2cl/min until the loss of righting reflex, as per APLAC guidelines at Stanford University. Immunization was performed by subcutaneous injection of the vaccine in the flanks of the mice, with the injection site changing every week. Mice were monitored weekly for early signs of auto-reactivity to the vaccine by weight measurements and gross examination of overall appearance. Vaccination preparation and dosage were the same for the prophylactic and adjuvant treatment experiments. The prophylactic vaccination studies were replicated several times in the same mouse strain, different mouse strains and by different investigators. The investigator analyzing the tumor sizes and data from the adjuvant treatment experiment was blinded for the different treatment groups.

Mixed lymphocyte reaction (MLR)

Spleens were isolated, minced, and filtered through a 70 μ m strainer. After multiple washes with glucose-containing RPMI, the pellet was resuspended in ACK lysis buffer for removal of red blood cells. CFSE-labeled (ThermoFisher Scientific) splenocytes from C+I vaccinated mice were then plated at a density of 1×10^5 cells per 100 μ l in a 96-well plate and incubated for 72 hr with another 100 μ L solution of DB7 tumor lysate, ranging from 1-10 μ g. After 72 hr, the plate was spun down and the supernatant isolated for cytokine analysis using the mouse Th1/Th2/Th17 Cytokines Multi-Analyte ELISArray kit (QIAGEN, Hilden, Germany), and the cell pellet was analyzed with the LSR-II Flow Cytometer to assess T cell proliferation.

IgG binding assay

Cells were washed multiple times with PBS and resuspended in 100 μ L FACS buffer with the addition of 2 μ L of serum from the vaccinated mice and incubated for 30 minutes on 4°C. Following this, cells were washed multiple times and incubated with an anti-IgG FITC secondary antibody (ThermoFisher Scientific) for another 20 min on 4°C. As an isotype control an IgG antibody, pre-adsorbed for murine IgG and IgM, was included. The cells were then analyzed using the LSR-II Flow Cytometer.

Histopathology of explanted organs

At time of sacrifice, the heart and kidneys were explanted from vaccinated mice and processed for histopathology. Briefly, the organs were fixed overnight in 4% paraformaldehyde and transferred to 70% ethanol for 24 hr. Fixed samples were embedded in paraffin and 5 μ m sections were cut and stained with hematoxylin and eosin (H&E) for histological analysis by a pathologist.

Isolation of inflammatory cells and serum from blood, spleen, tumor, and dLNs

FVB, C57BL/6, and CBA/J experimental mice were sacrificed at 4, 2, and 1 week(s), respectively, after tumor inoculation. Tissues were isolated from the mice and placed in a digestion buffer containing RPMI, FBS, collagenase, DNase, trypsin inhibitor and HEPES, then minced and placed in a shaker at 37°C for 45 min. Samples were then filtered through a 70 μ m strainer, spun down, and resuspended in ACK lysis buffer to remove any red blood cells. After lysis, the cell suspension was washed with PBS and used for subsequent analyses. Additionally, dissociated tumors were passed through a Percoll gradient to remove non-immune cells and isolate tumor-infiltrating leukocytes (TILs). Blood was collected in two separate tubes per mouse for PBMC (EDTA containing tube) and serum isolation (uncoated tube).

Staining of inflammatory cells for FACS analysis

Inflammatory cells isolated from blood and tissues were resuspended in 200 μ L FACS buffer (DPBS, 2% FBS and 200 μ M EDTA), blocked with a FcR-blocking Reagent (BD PharMingen, San Diego, CA, USA), and divided into 2 tubes. One tube was stained with a surface marker panel, containing CD3, CD4, CD25 (eBioscience), CD8a, CD44, CD45 (Biolegend), and the intracellular markers Granzyme-B (eBioscience) and FoxP3 (Biolegend). The second tube was stained for F4/80, MHC-II (eBioscience), CD86 (BD Biosciences), CD11b, CD11c, NK1.1, Ly6-G, and CD45 (Biolegend). A rat IgG2b κ isotype control was included for CD44, FoxP3 (Biolegend), and MHC-II (eBioscience). A rat IgG2a κ isotype was included for the Granzyme-B (eBioscience) and CD86 (BD Biosciences) staining. For CD25 staining, the IgG1 κ isotype (eBioscience) was included. In both panels, the fixable viability dye 780 (Invitrogen) was added to exclude dead cells from the analysis. Extracellular staining was performed prior to fixing and permeabilizing the samples for staining with intracellular markers. Samples were analyzed on the LSR-II Flow Cytometer analyzer in the Beckmann FACS facility (Stanford University).

Teratoma formation

Teratoma formation was performed as previously described (Nelakanti et al., 2015), with the exception of site of injection. For this manuscript, a flank injection was preferred over a hindlimb injection to ensure easier access for over-time measurements of teratoma size. In brief, 1×10^6 iPSCs were resuspended in growth factor reduced Matrigel (50 μ L per injection) and injected in

the flank of immunodeficient mice (NOD-SCID IL2Rgamma^{null};NSG). Teratoma sizes at site of injection were measured over time using a caliper. After four weeks, mice were sacrificed and the teratomas harvested for final measurements.

Generation of tumor lysate

1x10⁷ tumor cells were used from *in vitro* culture and resuspended in 1 mL of PBS. The cell suspension was frozen to –80°C for 45 min and then thawed on 37°C for 30 min. This process was repeated for a total of three times. Afterward, the suspension was spun down and the supernatant, containing tumor lysate, was isolated for protein concentration measurements using the Pierce BCA Protein Assay Kit (ThermoFisher Scientific).

Luminex multiplex cytokine assay

Production of various cytokines was measured in cell culture supernatant and serum samples using a multiplex-Luminex platform (LabMap200 System; Luminex) in conjunction with Panomics antibodies at the Human Immune Monitoring Center at Stanford University.

ELISPOT assay

Splenocytes (5x10⁵) were isolated as described above and co-cultured with either iPSC or DB7 lysate (35 µg) for the duration of 37 hr, after which the secretion of granzyme-β and IFN-γ was measured by Enzyme-Linked ImmunoSpot (ELISPOT) according to the manufacturer's instructions (cat# ELD5819, R&D Systems, Diaclone). Adobe Photoshop CS6 software was used for the calculation of size and number of IFN-γ positive spots.

Adoptive transfer of splenocytes and T cells

C+I vaccinated and vehicle vaccinated mice were sacrificed and their splenocytes isolated, as previously described (Galvan et al., 2015; Naas et al., 2010; Sodhi et al., 1985). In brief, the spleens were digested and passed through a 70 µm strainer. Afterward red blood cells were lysed with ACK lysis buffer (cat# 118-156-101, Quality biology, INC.) and the remaining splenocytes washed with PBS. The splenocytes were then dissolved in 200 µL PBS solution and intravenously injected in an orthotopic model of breast cancer by tail vein injection. For the adoptive transfer of T cells, the procedure is as described above, with the addition of a magnetic bead sorting using the Pan T cell isolation kit to acquire CD3⁺ T cells (#130-095-130, Miltenyi, Germany) after the final washing step.

Orthotopic tumor model

FVB mice were injected with 2x10⁶ DB7 tumor cells directly into the mammary fat pad tissue, as previously described (Kocatürk and Versteeg, 2015). The range of cancer cell number was based on previous reports (Chen et al., 2011; Evans et al., 2014) and was set at 2x10⁶ DB7 cancer cells after validating the model and achieving a tumor incidence of 100%.

Isolation of TELs from draining lymph nodes.

After sacrificing the C+I and vehicle-vaccinated mice, their dLNs were isolated, minced and passed through a 70 µm strainer. After washing the cells with PBS, the T cell portion of the TELs were isolated using the Pan T cell isolation kit to acquire CD3⁺ T cells (#130-095-130, Miltenyi, Germany).

Anti-nuclear antibody (ANA) ELISA

Murine blood was collected from PBS, CpG only, or CpG-iPSCs vaccinated mice and the plasma was separated from the blood via centrifugation for 15 min at 1000 g. The plasma samples were diluted at 1:200 with sample dilution. The concentrations of anti-nuclear antibodies (IgG) were determined using an ELISA kit, according to the manufacturer's instructions (Antibodies-Online; antibodies-online.com). For this experiment, four biological replicates per group were used and for each biological replicate three technical replicates were included.

Cytometry by Time of Flight (CyTOF)

Immune cells were isolated from explanted tissues according to aforementioned methods. Cells were stained with the Mouse Spleen/Lymph Node Phenotyping kit, the Mouse Intracellular Cytokine I Panel kit, and the viability dye Cisplatin (Fluidigm, South San Francisco, CA). Cells were resuspended in MaxPar water at a concentration of 1x10⁵-1x10⁸ cells per ml with the addition of normalization beads and ran on a CyTOF2 (Fluidigm) machine. Following this, the data were normalized using the normalization beads. The data were analyzed using the Cytobank online software for spanning tree progression analysis of density-normalized events (SPADE) (Qiu et al., 2011).

PCR detection of the large genomic deletion in *Cdkn2a*

Primers were designed to detect the junction of the large deletion in *Cdkn2a* of the B16 melanoma cell line (Figure S7B). Each 25 µl PCR reaction solution contained 1.25 units of PrimeSTAR® GXL DNA Polymerase (Clontech) and 50-100 ng of genomic DNA extracted by DNeasy Blood & Tissue Kit (QIAGEN) (Figure S7C). PCR products were then analyzed by Sanger sequencing and aligned with the gene database in NCBI (Figure S7D).

T cell Receptor (TCR) sequencing

The DNA from the TILs infiltrating the AC29 tumors was isolated using the DNeasy Blood & Tissue kit (QIAGEN). Samples were submitted to Adaptive Biotechnologies (Seattle, WA) for a survey level TCR sequencing. The minimum DNA content from the submitted samples was 150 ng per sample with DNA quality A260/280 between 1.8 to 2.0. Data analysis as well as assessment of TCR clonality between samples were performed in collaboration with Adaptive Biotechnologies. In brief, a list of TCR clones within each sample and their frequencies within the DNA sample were provided. For the T cell overlap search, the amino acid sequences of the clones appearing in 4 or 5 of the samples in the two sample groups were compared. Data from the CI treatment group and the PBS control group were ruled comparable with similar average productive unique values (PBS: 3582.2, CI: 3005.4).

QUANTIFICATION AND STATISTICAL ANALYSES

All values are expressed as mean \pm cs.d. or mean \pm cs.e.m. as indicated. Intergroup differences were appropriately assessed by either unpaired two-tailed Student's *t* test or one-way/two-way analysis of variance (ANOVA) with Tukey's posthoc test using PRISM GraphPad software. * $P < 0.05$, ** $P < 0.01$, *** $P < 0.001$, **** $P < 0.0001$.

Cluster identification, characterization and regression (Citrus)

In brief, based on hierarchical clustering and a regularized regression model, Citrus generates a list of stratifying clusters and behaviors from multidimensional data. In addition, it can describe their features (e.g., intracellular cytokines) and provide a predictive model for newly acquired data or validation samples. The stratifying features from these clusters were plotted as median expression on the x axis (Figures 5B, 7C, and S5B). CyTOF data were analyzed using Cytobank and gated for viable single cells, after which the FCS files were uploaded in the GUI from Citrus 0.8 and the script was run in R (version 3.0.3). For the analysis of the splenocytes exposed to B16F0 tumor lysate, Citrus analysis was performed with 10,000 sampling events with 0.2% (567 events) minimum clustering. For the TILs, Citrus analysis was based on 1,000 sampling events with 500 events minimum clustering. Clustering features were found to be of interest with a *cv.min* and *cv.fdr.constrained* of less than 25.

Quantification of tumor load for melanoma by digital droplet PCR (ddPCR)

Primers and probe were designed to detect 3 SNPs (colored in red) that are specific to the B16 melanoma cell line. DNA was extracted from the tumor resection area and dLNs of C57BL/6 mice four weeks after R1 tumor resection using the DNeasy Blood & Tissue Kit (QIAGEN). Each ddPCR reaction solution was reconstituted to a final volume of 20 μ L using 40 to 50 ng of DNA template and ddPCR Supermix for Probes, without dUTP (BioRad). Each sample was quantified by using 2 probes: MT probe to assess the tumor load, and TaqMan[®] Copy Number TFRC probe (Mm00000692_cn, ThermoFisher) to assess the cell amount (Figure S7E, F). The final primer and probe concentrations were 900cnM and 250cnM, respectively. Droplet formation was carried out using a QX100 droplet generator with 20 μ L of PCR reaction solution. A rubber gasket was placed over the cartridge and loaded into the droplet generator. The emulsion (35 μ L in volume) was then slowly transferred using a multichannel pipette to a 96-Well twin.tec PCR Plates (Eppendorf). The plate was then heat-sealed with foil and the emulsion was cycled to end point per the manufacturer's protocol with annealing temperature at 62.5°C. The samples were then read using a BioRad QX100 reader. The standard curve was created for different amounts of tumor load, including 0%, 1%, 5%, 10%, 25%, 50%, 75%, 90%, 95%, 99%, and 100%, and linear regression equation was utilized to quantify the tumor load for each DNA sample (Figure S7G). Following are the sequences of the primers and probes for detecting tumor load:

Forward primer, 5'ACTAGCCAGAGGATCTTAAAGACT3';

Reverse primer, 5'GCCATCACTGGAAAGAGAGGC3';

Mutant Probe, 5'(HEX)CCTGCCACCCACTCCCCCTTTT (Blackhole Quencher)3'; (red indicating mutant-specific alleles).

Analysis of RNA-sequencing data

The pair-end human RNA-seq data from normal and cancer cell lines were downloaded from the GEO repository of ENCODE project (<https://www.genome.gov/encode/>) (Consortium, 2011). The RNA-seq of iPSCs reprogrammed by different methods were generated from previous publication (Churko et al., 2017). The fastq files of the sequencing were aligned to the human genome (hg19) by Hisat (<https://ccb.jhu.edu/software/hisat/index.shtml>) (Kim et al., 2015). The aligned reads were assigned by HT-seq (<http://www-huber.embl.de/users/anders/HTSeq>) (Anders et al., 2015) to the gene annotation (version 19) provided by the GenCode project (<http://www.genecodegenes.org/>) (Harrow et al., 2012). The gene expression levels were estimated and normalized by DESeq (<https://bioconductor.org/packages/release/bioc/html/DESeq.html>) (Anders and Huber, 2010; Anders et al., 2013). The gene expression levels were extracted from a curated selection of cancer-related genes described in seven datasets (allOnco; Bushman Lab, University of Pennsylvania) after which a heatmap was generated using GENE-E (<https://www.broadinstitute.org/cancer/software/GENE-E>).

Analysis of murine RNA sequencing data

The pair-end/single-end RNA-seq data from tissues were downloaded from the mouse ENCODE project (<http://mouseencode.org/>). The mouse iPSC data were downloaded from GSE36294 (Chang et al., 2014). The fastq files of the sequencing were aligned to the mouse genome (mm10) by Hisat (<https://ccb.jhu.edu/software/hisat/index.shtml>). The aligned reads were assigned by HT-seq (<http://www-huber.embl.de/users/anders/HTSeq>) to the gene annotation (version M3) provided by the GenCode project (<http://www.genecodegenes.org/>). The gene expression levels were estimated and normalized by DESeq (<https://bioconductor.org/packages/release/bioc/html/DESeq.html>). The heatmap was generated using GENE-E (<https://www.broadinstitute.org/cancer/software/GENE-E>).

DATA AND SOFTWARE AVAILABILITY

T cell receptor sequencing data have been deposited in the immuneACCESS platform under the following accession number: <https://doi.org/10.21417/B7B648>.